NASA CONTRACTOR REPORT

NASA CR-338

NASA CR-338

ANALYTICAL RESEARCH ON A SYNCHRONOUS GYROSCOPIC VIBRATION ABSORBER

by William G. Flannelly and John C. Wilson

Prepared under Contract No. NASw-855 *by*
KAMAN AIRCRAFT CORPORATION
Bloomfield, Conn.
for

NATIONAL AERONAUTICS AND SPACE ADMINISTRATION - WASHINGTON, D. C. - DECEMBER 1965

NASA CR-338

ANALYTICAL RESEARCH ON A SYNCHRONOUS GYROSCOPIC VIBRATION ABSORBER

By William G. Flannelly and John C. Wilson

Prepared under Contract No. NASw-855 by
KAMAN AIRCRAFT CORPORATION
Bloomfield, Conn.

for

NATIONAL AERONAUTICS AND SPACE ADMINISTRATION

For sale by the Clearinghouse for Federal Scientific and Technical Information
Springfield, Virginia 22151 - Price $3.00

TABLE OF CONTENTS

TABLE OF CONTENTS (Continued)

LIST OF FIGURES

LIST OF FIGURES (Continued)

LIST OF SYMBOLS

a	Effective barrel length in structural flexibility representation (see Figure 13)
a_n	Fourier coefficient
A_0-A_3	Stability quartic equation coefficients
b	Effective barrel length in structural flexibility representation (see Figure 13)
b_n	Fourier coefficient
C	Vector representation or damping coefficient
f_A	Antiresonant frequency
F	Force
F_o	Maximum amplitude of force
h	Distance from pivot to center of mass on the Coriolis Absorber
I	Moment of inertia
K	Spring constant
K_1, K_2	Integration constants
ℓ	Distance from pivot, X_4, to center of gravity of tare mass, i.e. yoke and nonrotating part of gyro disc
m	Total mass of GVA, including disc and supporting structure
m_b	Mass of GVA barrel
m_d	Mass of GVA rotor (i.e. disc)
m_T	Mass of GVA tare (i.e. yoke and nonrotating part of gyro disc
M_e	Effective mass of structure at point of GVA attachment

LIST OF SYMBOLS (Continued)

M_T	Total mass, including effective mass and GVA mass
r	Distance from pivot to center of gravity of barrel
a	Distance from pivot to center of gravity of disc
a_1	Ratio of (static) first mass moment to mass of GVA
S	(Static) first mass moment of GVA about attachment pivot
W	Weight of GVA
Z_q	Displacement impedance
α	Dissipation energy in large angle GVA solution
δ	Displacement of structure with absorber
δ_o	Displacement of structure without absorber
δ_1	Maximum displacement amplitude in large angle solution
$\eta \cdot \eta_4$	Parallel GVA stability equation components
ζ	Damping ratio, $\frac{C}{2I\omega_q}$
θ	Nutational angle
μ	Mass ratio, $\frac{m}{M_e}$
ϕ	Precessional angle
ψ	Gyro rotation angle
ω	Excitation frequency
Ω	Rotational velocity

LIST OF SYMBOLS (Continued)

Subscripts

d	Rotor disc of GVA
p	Principal axes designation
f	Fixed axes designation
α	Angular motion due to structural flexibility

ANALYTICAL RESEARCH ON

SYNCHRONOUS GYROSCOPIC VIBRATION ABSORBER

SUMMARY

12160

The feasibility of a synchronous dynamic vibration absorber based on gyroscopic resonance is demonstrated analytically and experimentally. The linearized equations of motion are solved for response of the body to which the absorber is attached as a function of excitation frequency, gyro speed, excitation force, and gyro configuration characteristics. A method of solving the nonlinearized equations is presented. Because of the excitation synchronization possible, the superiority of the gyroscopic absorber over the conventional Frahm absorber is demonstrated. For a parallel arrangement of two gyroscopic absorbers, one damped and one undamped, both an undamped antiresonant frequency and a damped resonant frequency are obtained.

The effects of elastic restraint, damping, and flexibility in the support structure were examined analytically. Analysis indicates the feasibility of simultaneous synchronization of an absorber to two excitation frequencies and isotropic absorption in the plane of rotation.

INTRODUCTION

In vehicles and machines which are subjected to vibratory forces of constant frequency, conventional dynamic vibration absorbers (of the type invented by H. Frahm in 1909) have been used with great success. When the frequency of the exciting force varies even slightly, the conventional dynamic absorber must be heavier than the weight necessary to meet force-level and tuning requirements, because the frequency bandwidth of significant attenuation, which is a function of the mass of the absorber, must be then wide enough to cover the range of excitation frequency. If the excitation frequency varies more than a few per cent, a conventional dynamic absorber of tolerable weight is likely to do more harm than benefit.

All rotating machinery produce vibratory forces on the supporting structure. The frequency of these excitations are harmonics of the rotational frequency. In some instances, such as the case of a very accurately, but not perfectly, balanced gyroscope, the excitation forces are small. In cases like the helicopter and screw-driven ocean vessel, the excitations are usually quite large. In almost all cases of rotating machinery, the excitation frequency varies at least a few per cent. In many cases, such as ocean vessels and certain compound aircraft, the excitation frequency will vary to such a degree that conventional dynamic absorbers are impractical.

Figure 1 shows the dynamic response of a structure with one natural frequency. The structure undergoes a resonance when the excitation frequency coincides with the natural frequency. In Figure 2, the effect of attaching a conventional dynamic absorber to the structure is shown. The absorber creates an antiresonance for one particular frequency, but it adds another degree of freedom to the system, and therefore adds another natural frequency. Unless the excitation is restricted to a very narrow range about the antiresonance, the addition of the absorber results in two potentially serious amplifications instead of one (Reference 1).

Figure 3 illustrates a different concept in structural vibration absorption: the structural Frequency Response Curve is made to be a function of the RPM of the excitation machinery and varies in such a manner that the antiresonance frequency coincides with the excitation frequency. This results in very nearly 100 per cent absorption at virtually all RPM. The frequency at which the Gyroscopic Vibration Absorber is the most effective is a function of the speed of the gyro wheel. As a result, the gyro speed may be synchronized directly to the excitation frequency.

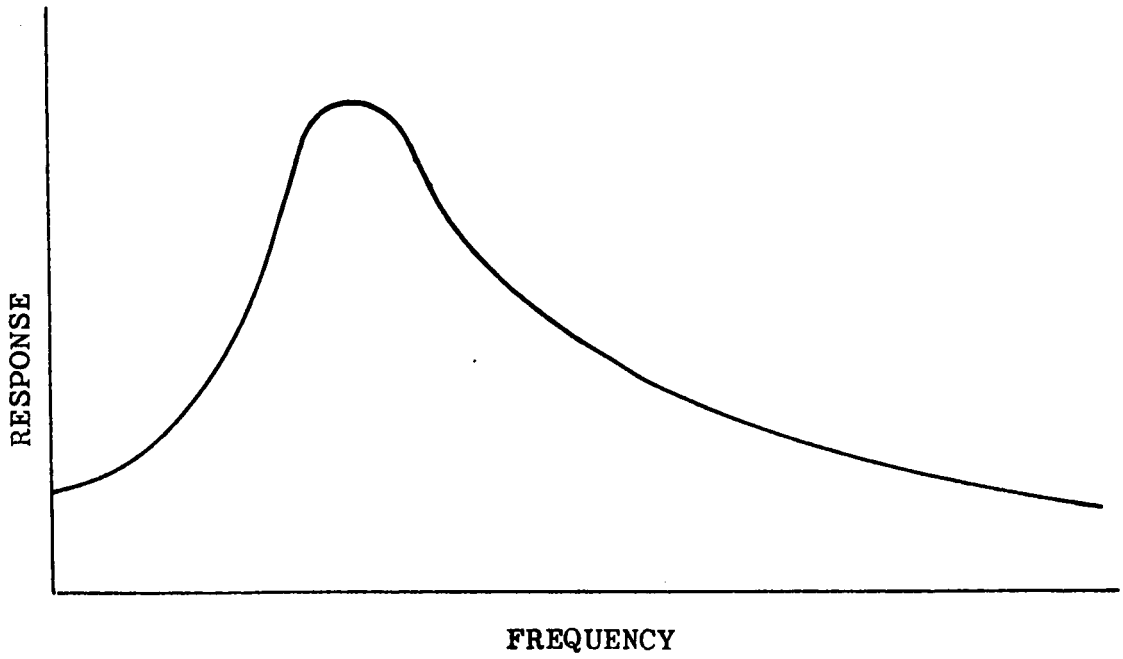

FIGURE 1.- GENERAL RESPONSE OF A STRUCTURE
WITHOUT A VIBRATION ABSORBER

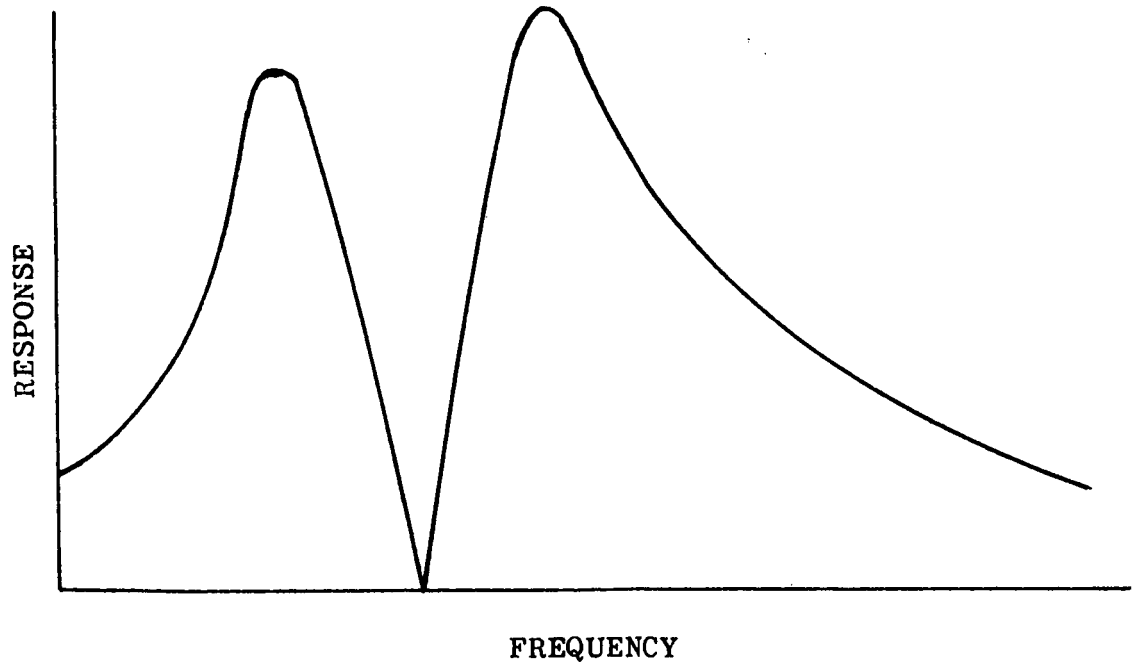

FIGURE 2.- GENERAL RESPONSE OF A STRUCTURE
WITH A CONVENTIONAL VIBRATION ABSORBER

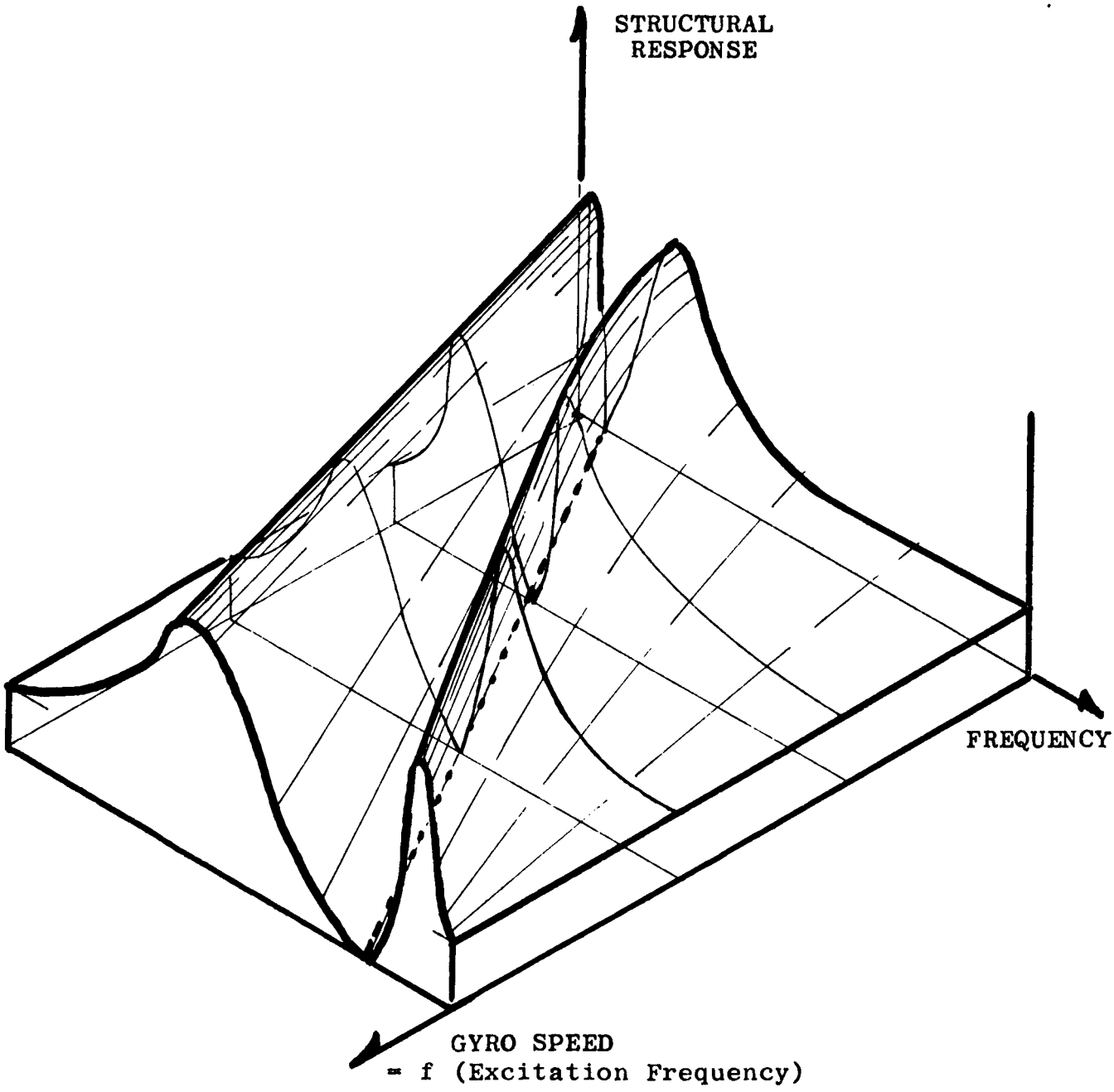

FIGURE 3. - GENERAL RESPONSE OF A
STRUCTURE WITH SYNCHRONOUS VIBRATION ABSORBER

In this report, the analytic principles of the synchronous gyroscopic vibration absorber are established. The analysis is directed toward accurate description of the pertinent equations of motion. Linearization of these equations with the assumption of small angular motion is accomplished. As well, the restriction to small angles is removed for an alternate solution of the resulting nonlinear equations. There is considered the effects of damping and spring restraint. The primary characteristic sought was the response of a body to which the absorber is attached as a function of the excitation frequency, gyro speed, the ratio of force/mass, damping, elastic restraint and absorber mass/effective mass ratio.

Derivation of the equations of motion was accomplished by Lagrangian methods. The linearized solution of the Gyroscopic Vibration Absorber (GVA) equations, without synchronization, was compared to the characteristic response of the Frahm absorber. In addition, a linearized solution of equations of motion for a combination of two gyroscopic absorbers mounted in parallel was obtained and compared with a similar Frahm combination. In both combinations, only one, i.e. Frahm or GVA, was damped.

A method of solving the large angle equations of motion was contributed by Dr. Howard W. Butler, Chairman of the Department of Mechanical Engineering at West Virginia University and formerly of the Hartford Graduate Center of Rensselaer Polytechnic Institute. Mr. Roland Anderson and Mr. Michael Smith participated in the derivation of the equations of motion and the solution of the linearized equations.

DISCUSSION OF DYNAMIC ABSORBERS

The Frahm Absorber

The spring-mass dynamic vibration absorber, invented by H. Frahm in 1909, is successfully used, in a wide variety of applications, to modify the dynamic response of structures in such a manner that an essentially infinite impedance (zero response) is created at the attachment point of the absorber for a particular, predetermined frequency. When the excitation frequency on any machine or structure is not constant, or very nearly so, the Frahm absorber is ineffective and may, because of the resonant condition it adds to the system, do more harm than good (Reference 1). The frequency bandwidth, across which the Frahm absorber is significantly effective, is a function of the ratio of the absorber mass to the "effective mass" of the structure to which it is attached. Because excitation frequencies almost always vary at least a few per cent, most vibration absorbers in use in aircraft today must be several times heavier than the minimum weight, dictated by force-level and tuning requirements, to adequately cover the excitation bandwidth (Reference 2).

The function of an undamped dynamic absorber is to react the effective excitation force, at the attachment point of the absorber, and not (contrary to what its name seems to imply) to "absorb" a certain amount of "vibratory energy" from the structure. The maximum force which a Frahm absorber can react is determined by the allowable stress in its spring, the spring stiffness and the maximum deflection. However, the antiresonant frequency is given by the ratio of the absorber spring stiffness to absorber mass. It is readily appreciated that the designer of a Frahm absorber often has a difficult task striking a reasonable balance between the stress, stiffness and minimum weight requirements for given force level and antiresonant frequency.

The ineffectiveness of the Frahm absorber at any but a single, nearly constant excitation frequency; the necessity for additional absorber weight to give a practical, although still narrow bandwidth; and the inherent design limitations necessitated by the potential energy portion of the absorber, motivated a search for a purely kinetic dynamic absorber having a remotely controllable and linearly synchronizable antiresonant frequency. This search resulted in the Gyroscopic Vibration Absorber.

Linear Synchronous Absorbers

While synchronous absorbers have been used in torsional systems (Reference 1) for many years, the out-of-plane centrifugal pendulum (References 8, 9, and 10) is the only synchronous absorber for general use in linear vibrations other than the GVA. The only reference in the literature known to the authors, which discusses actual experiments with this absorber (Reference 10) indicates that the device was not successful. It might be logically presumed that friction from centrifugal loading of the pendulum pivots contributed to the lack of success in the experiment, although this is conjecture. One of the objectives in the design of the GVA was to avoid a large steady radial load (such as centrifugal force) on the oscillatory pivots.

The out-of-plane centrifugal pendulum absorber is quite space-consuming for aircraft applications, compared to the GVA, and would produce undesirable moments (assuming it can be made to work) in installations which would require cantilevering the device from structure. In the opinion of the authors, the centrifugal pendulum absorber can be made to work and would be most useful in certain applications.

The in-plane centrifugal absorber (References 9 and 10) has been successfully applied in helicopter experiments, but, as the in-plane type can cause potentially destructive mechanical instability unless very prudently applied, its use is restricted, for practical reasons, to highly specialized applications such as in-plane excitations on helicopter rotor heads. This absorber has not been applied to any helicopters in actual use.

The out-of-plane centrifugal pendulum absorber was discarded by the senior author, in his original search for a suitable aircraft structural synchronous absorber, largely because of space requirements, mounting difficulties and the stress and friction problems resulting from steady centrifugal loading. The in-plane centrifugal pendulum absorber was discarded in consideration of the danger of destructive mechanical instability (which is a function of the aircraft structural impendance), in addition to the reasons mentioned above for the out-of-plane case.

The Gyroscopic Vibration Absorber

The Gyroscopic Vibration Absorber, shown schematically in Figure 4, is a completely inertial, conservative means of reacting a sinusoidal force. A natural frequency in the decoupled GVA is achieved through an oscillating flow of energy between the precessional and nutational kinetic states of the gyroscopic disc which is analogous to the more common case of the elastic-inertial system in which the energy flows between the potential energy and kinetic energy states. The antiresonant frequency of the GVA is, for small precessional and nutational angles, linearly proportional to the angular velocity of the gyroscopic disc. If the disc velocity is properly synchronized to the frequency of a sinusoidal excitation, the GVA will produce an antiresonance on the structure at all values of the excitation frequency, thereby producing the effect of theoretically infinite bandwidth as regards the excitation to which the GVA is synchronized (see Figure 3).

Helicopters, compound aircraft, rotary wing spacecraft decelerators, and certain VTOL aircraft are usually excited primarily by the nth harmonic of the rotational speed of the N-bladed rotor or propeller. Almost all vehicles, from rockets to railroad cars are subjected to some excitation which is a harmonic of the speed of rotating machinery, such as wheels, pumps, actuators, etc. Synchronization of the GVA to such discrete harmonics is uncomplicated, involving only an open-loop means of driving the gyroscopic disc at a speed which is a multiple of the speed of the disturbing machinery.

It is conceivable that the GVA antiresonant frequency could be synchronized to the frequency of the worst disturbance in a distributed excitation spectrum using circuitry which would pass only input signals above a certain predetermined magnitude and select a synchronization frequency within the bandwidth of the greatest disturbance. Before such a scheme would be of practical value, it is necessary to attenuate the resonant response of the GVA without deterioration of the antiresonant effectiveness; a means for accomplishing this was found in the course of this research, and it is reported in the section titled "Parallel GVA Mounting". However, in light of the serious, more immediately practical problem of discrete harmonic disturbance, the matter of absorption of purely distributed, or so-called random, excitation is of secondary concern in this project.

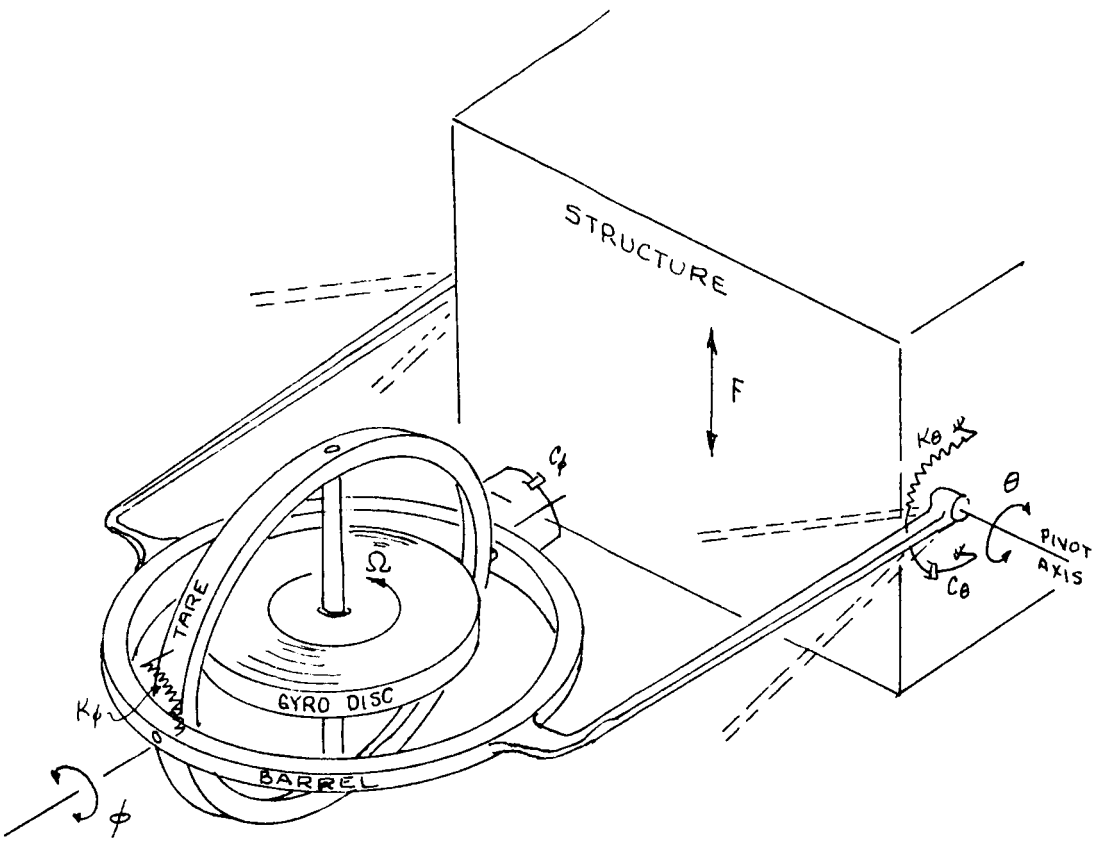

FIGURE 4.- GENERAL CONFIGURATION OF THE GYROSCOPIC VIBRATION ABSORBER

The "Parallel GVA Mounting" scheme appears to be a practical solution to the quite realistic problem of an excitation environment consisting of a very high discrete harmonic disturbance along with a lower magnitude, but not insignificant, distributed disturbance spectrum.

Aside from the obvious use of the GVA as a synchronous dynamic absorber, the ability which it gives to remotely control and change the dynamic properties of a structure through control of the angular velocity of a gyroscope could have significant uses in research and testing. The desirability of remote control of the dynamic properties of structures undergoing flutter or buffeting, for example, was mentioned in 1955 by Thompson and Yeates of NACA (Reference 3).

The basic features of the Gyroscopic Vibration Absorber, along with the additional properties of planar isotropy and simultaneous synchronization to two excitations, may be found in an alternate configuration which is analytically described in the section titled "Coriolis Absorber Configuration".

EQUATIONS OF MOTION

Description of the System

The Gyroscopic Vibration Absorber is shown schematically in Figure 4, mounted to vibrating structure. The absorber consists of three primary parts:

(1) The Gyroscopic Disc which spins at constant angular velocity, Ω, relative to its shaft. The Gyroscopic Disc would, most likely, contain the field coil of the driving motor.

(2) The Tare consists of the shaft, the motor armature, and the inner gimbal frame or yoke. The Tare oscillates through angle θ and angle ϕ.

(3) The Barrel, or outer gimbal frame, oscillates through angle θ about a pivot axis on the structure. The pivot (θ) axis is perpendicular to the ϕ axis and does not intersect the center of gravity of the absorber.

The Gyroscopic Vibration Absorber does not require elastic restraint or dissipative devices to perform its primary function. However, springs and dampers are shown about the θ and ϕ axes in Figure 4, and are included in some of the analyses to account for elastic and dissipative effects which cannot be entirely eliminated in any practical device, and to examine the effect of deliberately incorporated pivot springs and dampers on absorber performance.

The structure to which the Gyroscopic Absorber is mounted is represented as an effective mass only in Figure 4. Because only narrow antiresonant frequency bandwidths are of interest (due to the very nature of the synchronous absorber) in the following analyses, the slope of the structural impedance across the bandwidth will generally be nearly constant. As an arbitrary basis for comparative analysis of various configurations of gyroscopic absorbers and Frahm (spring-mass) absorbers, the magnitude and slope of basic structural impedance is set equal to the magnitude and slope of an arbitrary mass, M_e. This appears to be a less restrictive basis of comparison of dynamic absorbers than the more common assumption that the basic structure is in resonance with the excitation frequency.

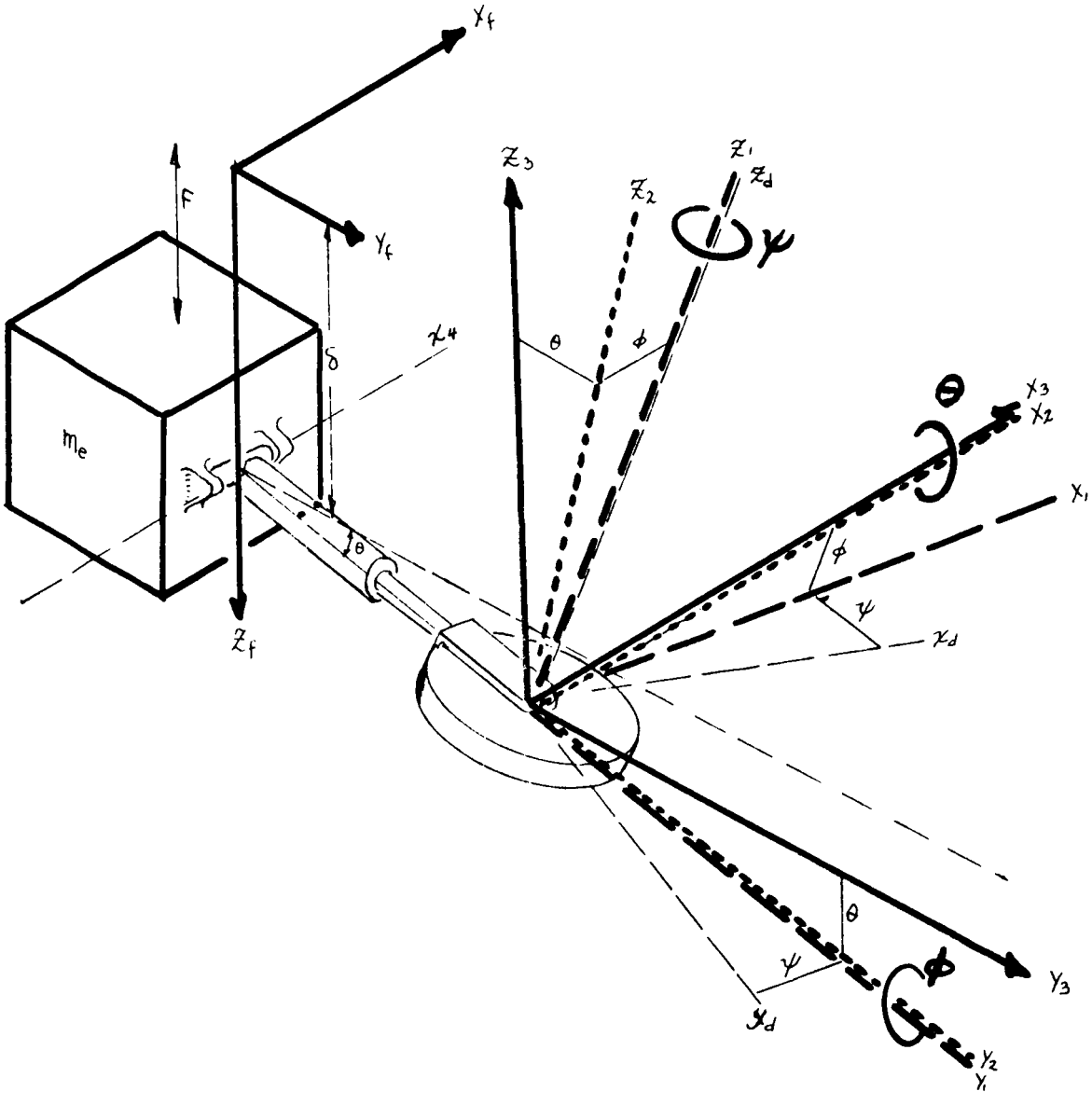

FIGURE 5.- DIAGRAM OF THE GVA

Derivation Of Equations

In Figure 5, consider a point mass (dm) on the gyro rotor and transfer the coordinates to a fixed space (inertial system). Consider axes X_d, Y_d, and Z_d fixed to the gyro rotor with Z_d as the axis of spin. The axes X_d, Y_d, and Z_d are rotated through angles Ψ, Φ, and Θ in that order to become axes X_3, Y_3, and Z_3 which are parallel to the fixed axes X_f, Y_f, and Z_f.

Using position tensors:

$$\begin{vmatrix} X_3 \\ Y_3 \\ Z_3 \end{vmatrix} = [\Theta][\Phi][\Psi] \begin{vmatrix} X_d \\ Y_d \\ Z_d \end{vmatrix} \tag{1}$$

where:

$$[\Theta] = \begin{bmatrix} 1 & 0 & 0 \\ 0 & \cos\theta & -\sin\theta \\ 0 & \sin\theta & \cos\theta \end{bmatrix} \tag{2}$$

$$[\Phi] = \begin{bmatrix} \cos\phi & 0 & -\sin\phi \\ 0 & 1 & 0 \\ \sin\phi & 0 & \cos\phi \end{bmatrix} \tag{3}$$

$$[\Psi] = \begin{bmatrix} \cos\psi & -\sin\psi & 0 \\ \sin\psi & \cos\psi & 0 \\ 0 & 0 & 1 \end{bmatrix} \tag{4}$$

The mathematical work will be simplified if, instead of using Lagrange's Equation directly, use is made of d'Alembert's Principle in the form employed in the derivation of Lagrange's Equation. This avoids the unnecessary algebraic labor of writing the actual Kinetic Energy Expression, and this process may be regarded as

rigorous employment of the Virtual Work Principle. Representing the vector $\begin{vmatrix} X_j \\ Y_j \\ Z_j \end{vmatrix}$ by $|C|$, d'Alembert's Equations for integration of a particle mass become:

$$\int \left[\frac{\partial C}{\partial \phi}\right]^T \left[\ddot{C}\right] dm = M_\phi \tag{5}$$

$$\int \left[\frac{\partial C}{\partial \theta}\right]^T \left[\ddot{C}\right] dm = M_\theta \tag{6}$$

It is seen from the derivation of Lagrange's Equation that the parallel axes transformation and the effects of the tare and barrel can be brought into the analysis by superposition upon the Euler-type rotation.

Choosing X_d, Y_d, and Z_d at the center of gravity of the disc, giving the disc polar symmetry, and letting Y_1 be a principal axis of the tare and barrel, the equations may be integrated to give the following equations of motion of the Classical Gyroscope configuration of the GVA.

Products of inertia were eliminated by representing such coefficients in terms of sums and differences of principal moments of inertia. The presence of periodic coefficients as expected is notable.

$$\begin{aligned} 0 = {} & \ddot{\theta}\left[I_{xd} + (I_{zd} - I_{xd})\sin^2\phi + \ell^2 m_d + I_{x4T} + I_{x4b}\right] + I_{zd}\Omega\dot{\phi}\cos\phi \\ & + 2\dot{\phi}\dot{\theta}(I_{zd} - I_{xd})\sin\phi\cos\phi + \ddot{\delta}(\ell m_d \cos\theta + \ell m_T \cos\theta) + K_\theta\theta + C_\theta\dot{\theta} \end{aligned} \tag{7}$$

$$0 = \ddot{\phi}(I_{xd} - I_{y1T}) - I_{zd}\Omega\dot{\theta}\cos\phi + \dot{\theta}^2(I_{xd} - I_{zd})\sin\phi\cos\phi + K_\phi\phi + C_\phi\dot{\phi} \tag{8}$$

$$\begin{aligned} F_o \sin\omega t = {} & \ddot{\delta}(m_d + m_b + m_r + Me) + \ddot{\theta}(\ell m_d + \ell m_T + r m_b)\cos\theta \\ & - \dot{\theta}^2(\ell m_d + \ell m_T + r m_b)\sin\theta \end{aligned} \tag{9}$$

SOLUTIONS TO EQUATIONS

Small Angular Motion

Discussion. - It may be seen by inspection that Equations (7), (8), and (9) may be closely approximated by linear equations for small values of θ and ϕ. This requires, then, that the precessional and nutational angles be limited to a maximum of on the order of 15 or 20 degrees. The resulting linearized equations in the following sections will describe the response of the structure to which the absorber is attached, as well as the corresponding precessional and nutational amplitudes of the GVA.

Linearized Equations. - Giving the gyroscopic disc polar symmetry about the axis of rotation ($I_{xd} = I_{yd}$), Equations (7), (8), and (9) become, for small values of θ and ϕ

θ Equation:

$$I_\theta \ddot{\theta} + I_z \Omega \dot{\phi} + S\ddot{\delta} + C_\theta \dot{\theta} + K_\theta \theta = 0 \tag{10}$$

ϕ Equation:

$$I_\phi \ddot{\phi} - I_z \Omega \dot{\theta} + C_\phi \dot{\phi} + K_\phi \phi = 0 \tag{11}$$

δ Equation:

$$M_T \ddot{\delta} + S\ddot{\theta} = F \tag{12}$$

where:

$$I_\theta = I_{xd} + s^2 m_d + I_{xdT} + I_{xdb}$$

$$I_\phi = I_{yd} + I_{yIT}$$

$$S = s m_d + \ell m_T + r m_b$$

$$M_T = M_e + m_d + m_T + m_b$$

Assuming a steady state solution of the form $q = Qe^{i\omega t}$, the small angle equations are, in matrix form,

$$\begin{bmatrix} -\omega^2 S & -\omega^2 I_\theta + K_\theta + i\omega C_\theta & i\omega I_z \Omega \\ 0 & -i\omega I_z \Omega & -\omega^2 I_\phi + K_\phi + i\omega C_\phi \\ -\omega^2 M_T & -\omega^2 S & 0 \end{bmatrix} \begin{vmatrix} \delta \\ \theta \\ \phi \end{vmatrix} = \begin{vmatrix} 0 \\ 0 \\ F \end{vmatrix} \qquad (13)$$

Using Cramer's Rule on the characteristic determinant, the displacement impedance of the basic structure is seen to be:

$$Z_a = \frac{F}{\delta} = \frac{\omega^4(S^2 I_\theta - M_T I_\theta I_\phi) + i\omega^3(M_T I_\phi C_\theta + M_T I_\theta C_\phi - S^2 C_\phi) + \omega^2(M_T I_\phi K_\theta + M_T I_\theta K_\phi + M_T C_\theta C_\phi + M_T I_z^2 \Omega^2 - S^2 K_\phi) - i\omega(M_T K_\theta C_\phi + M_T K_\phi C_\theta) - \omega^2(M_T K_\theta K_\phi)}{\omega^4(I_\theta I_\phi) - i\omega^3(I_\theta C_\phi + I_\phi C_\theta) - \omega^2(I_\theta K_\phi + I_\phi K_\theta + I_z^2 \Omega^2 + C_\theta C_\phi) + i\omega(K_\theta C_\phi + K_\phi C_\theta) + K_\theta K_\phi} \qquad (14)$$

With $C_\theta = C_\phi = K_\theta = K_\phi = 0$, the denominator in Equation (14) goes to zero, causing the structural displacement δ to be zero when

$$\boxed{\omega_a = \frac{I_z \Omega}{\sqrt{I_\theta I_\phi}}} \qquad (15)$$

the antiresonant frequency. It is especially important to note that ω_a is linearly proportional to Ω. If there is a discrete, but variable excitation frequency ω_x to which Ω can be so synchronized that

$$\Omega = \frac{\sqrt{I_\theta I_\phi}}{I_z} \omega_x \qquad (16)$$

The structure will exhibit zero response regardless of the value of ω_x. If, in a 3-bladed compound helicopter, for example, the ratio of the number of poles in a tachometer generator to the number of poles in the GVA synchronous motor is equal to $\frac{3\sqrt{I_\theta I_\phi}}{I_z}$, a GVA mounted on the compound helicopter would absorb all the predominant 3P excitation (at the absorber attachment point) in spite of large changes in rotor speed.

When the numerator in Equation (14) goes to zero, the resonant condition with the GVA is given by

$$\omega_R = \omega_a \sqrt{\frac{1+\mu}{1+\mu\left(1-\frac{I_z^2}{I_\theta^2}\right)}} \qquad (17)$$

The characteristic determinant can be used as well to calculate the amplitude of the precessional and nutational motion with the intent that these are to be limited to 20 degrees. For no damping or spring restraint, these angles are given by

$$\Theta = \frac{S I_\phi F_o}{I_\phi [S^2 - M_T I_\theta] \omega^2 + I_z^2 \Omega^2 M_T} \tag{18}$$

$$\phi = \frac{-i I_z S \Omega F_o}{I_\phi [S^2 - M_T I_\theta] \omega^3 + I_z^2 \Omega^2 M_T \omega} \tag{19}$$

Dividing one equation by the other yields:

$$\frac{\phi}{\Theta} = \frac{-i I_z \Omega}{I_\phi \omega} \tag{20}$$

and it is seen that $\phi > \Theta$.

By substituting Equation (15) into Equation (19), there is obtained

$$\phi = \frac{F_o}{\omega^2 S} \sqrt{\frac{I_\theta}{I_\phi}} \tag{21}$$

Bandwidth Comparison of GVA and Frahm Absorbers. - The structural displacement impedance at the attachment point (θ axis in Figure 5) of an unsynchronized GVA, without damping or spring restraint, and acting on a structure of acceleration - impedance, M_e, follows from Equation (14):

$$Z_d = \frac{F}{\delta} = \frac{\omega^4 \left(\frac{S^2}{I_\theta} - M_e - m \right) + \omega^2 \omega_a^2 (M_e + m)}{\omega^2 - \omega_a^2} \tag{22}$$

Rewriting Equation (22) in terms of the ratio of structural displacement without an absorber (δ_o) and the displacement with a GVA (δ) gives:

$$\frac{\omega_\delta^2}{\omega_a^2} = \frac{1 + \frac{\delta}{\delta_o}(1+\mu)}{1 + \frac{\delta}{\delta_o}\left[1 + \mu\left(1 - \frac{A^2}{\theta^2}\right)\right]} \tag{23}$$

Equation (23) requires some interpretation. ω_G/ω_a is the frequency (in per cent of ω_a) at which the structure, with an unsynchronized GVA, will have a displacement which is δ/δ_o times the displacement it would have without an absorber. Obviously, ω_G/ω_a is double-valued, as is readily deduced from Figure 6; it appears to be single-valued in Equation (23), only because the phasing of δ to δ_o (0^o to 180^o in the undamped case) is implicit. rewriting Equation (23) in terms of the absolute values of δ/δ_o yields two equations:

$$\frac{\omega_{GU}^2}{\omega_a^2} = \frac{1 + \left|\frac{\delta}{\delta_o}\right|(1+\mu)}{1 + \left|\frac{\delta}{\delta_o}\right|\left[1+\mu\left(1-\frac{\Delta_i^2}{\rho_\theta^2}\right)\right]} \tag{24}$$

and

$$\frac{\omega_{GL}^2}{\omega_a^2} = \frac{1 - \left|\frac{\delta}{\delta_o}\right|(1+\mu)}{1 - \left|\frac{\delta}{\delta_o}\right|\left[1+\mu\left(1-\frac{\Delta_i^2}{\rho_\theta^2}\right)\right]} \tag{25}$$

where ω_{GU} represents the upper frequency for a given value of $|\delta/\delta_o|$, and ω_{GL} represents the lower frequency at which the same value of δ/δ_o will be found. See Figure 6.

A similar calculation may be made for a Frahm absorber, shown in Figure 7. The upper frequency at which the structural response will be δ/δ_o times the response without an absorber is given by:

$$\frac{\omega_{FU}^2}{\omega_a^2} = \frac{1 + \left|\frac{\delta}{\delta_o}\right|(1+\mu)}{1 + \left|\frac{\delta}{\delta_o}\right|} \tag{26}$$

and the lower limit by:

$$\frac{\omega_{FL}^2}{\omega_a^2} = \frac{1 - \left|\frac{\delta}{\delta_o}\right|(1+\mu)}{1 - \left|\frac{\delta}{\delta_o}\right|} \tag{27}$$

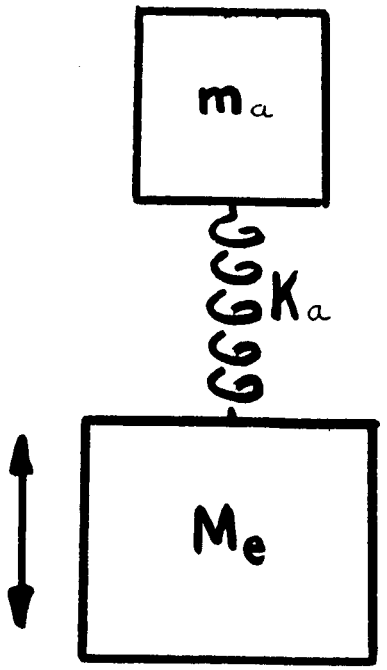

FIGURE 7.- FRAHM ABSORBER

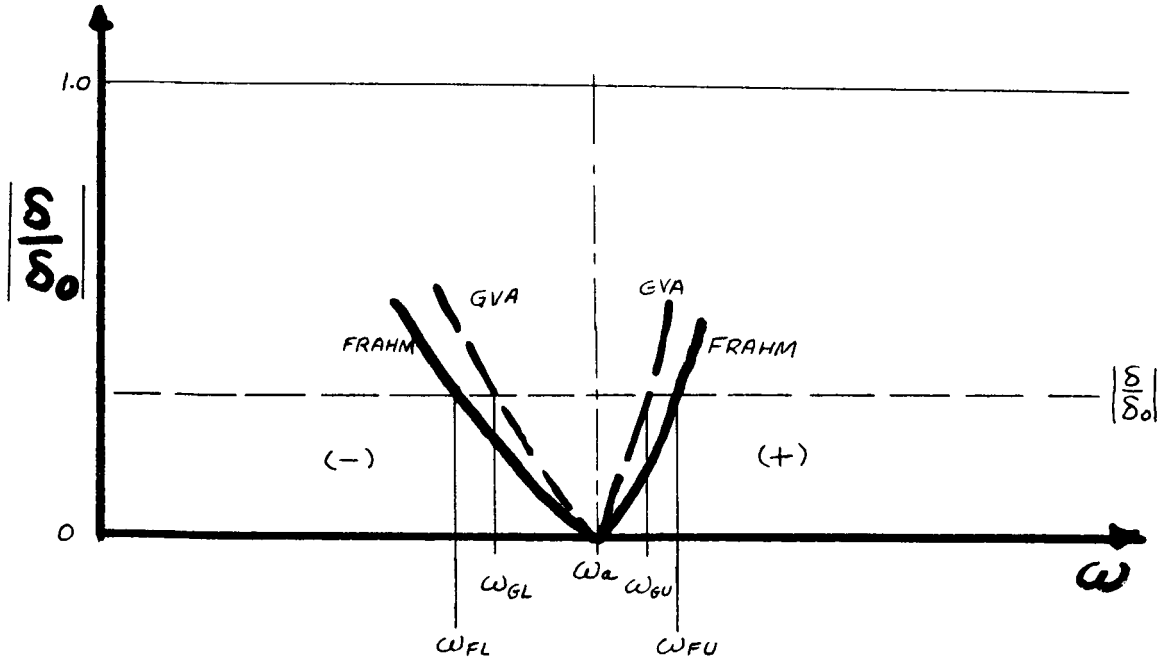

FIGURE 6.- BANDWIDTH COMPARISON OF GVA AND FRAHM ABSORBERS

Comparison of Equation (24) to Equation (26) and Equation (25) to Equation (27) shows that the bandwidth of the unsynchronized GVA is narrower than that of the Frahm. It should also be noted that the GVA cannot be reduced to the Frahm: Equation (24) can be made equal to Equation (26), for example, only when $\ell_1/\rho_\theta = 1.0$, a value which is quickly approached as the arm length ℓ_1 is increased.

While the bandwidth of the GVA is narrower than that of the Frahm, it is not necessarily very much narrower. In any case, the synchronization feature of the GVA makes bandwidth a secondary consideration, i.e. it need be only wide enough to cover synchronization error.

Damping. - While the effect of damping on the θ axis of the GVA might be expected to have effects similar to damping in the Frahm absorber, the exact effect of precessional (ϕ) damping in the GVA was not intuitively obvious. The following analysis shows that ϕ damping is the same in kind, although not in magnitude, as θ damping and damping about either the θ or ϕ axes produces effects similar to damping in the Frahm absorber.

From Equation (14), the following expression may be obtained for a structure (represented by mass M_e) equipped with a GVA having damping on the θ axis only, and having no pivotal elastic restraint:

$$\left|\frac{\delta}{\delta_0}\right|^2 = \frac{\left[\frac{\omega^2}{\omega_a^2} - 1\right]^2 + 4\frac{\omega^2}{\omega_a^2}\zeta_\theta^2}{\left[\frac{\omega^2}{\omega_a^2}\left(1 - \mu - \mu\frac{\ell_1^2}{\rho_\theta^2}\right) - (1+\mu)\right]^2 + 4\frac{\omega^2}{\omega_a^2}\zeta_\theta^2(1+\mu)^2} \qquad (28)$$

Similarly, the response equation for an unrestrained GVA with damping on the ϕ axis defined as the precessional axis is:

$$\left|\frac{\delta}{\delta_0}\right|^2 = \frac{\left[\frac{\omega^2}{\omega_a^2} - 1\right]^2 + 4\frac{\omega^2}{\omega_a^2}\zeta_\phi^2}{\left[\frac{\omega^2}{\omega_a^2}\left(1 + \mu - \mu\frac{\ell_1^2}{\rho_\theta^2}\right) - (1+\mu)\right]^2 + 4\frac{\omega^2}{\omega_a^2}\zeta_\phi^2\left(1 + \mu - \mu\frac{\ell_1^2}{\rho_\theta^2}\right)} \qquad (29)$$

The expressions are seen to be identical except for the second term in the denominator. It can be seen as well that the minimum response will shift away from the "antiresonant" frequency as damping increases, but is still proportional to gyro speed.

Figures 8 through 10 further demonstrate the similarity of response for the Frahm, θ damped GVA, and ϕ damped GVA. A mass ratio of 10 was chosen to make the bandwidth distinctive. As mass ratio increases, the bandwidth narrows. The distance between gyro disc center and attachment point was chosen to be four times the disc radius as typical. It can be seen that bandwidths are quite similar, and the effect of damping on all three devices is similar. It is also apparent that although the damping reduces the response at resonance, more importantly it increases the amplitude of minimum response. Therefore, it is concluded that the GVA should be nearly undamped in precession and nutation for best performance.

Elastic Restraint. - For an undamped GVA with elastic restraint about the nutational, θ, axis, the antiresonant frequency is simply derived from the General Equation as:

$$\omega_A^2 = \omega_\theta^2 + \frac{I_z^2 \Omega^2}{I_\theta I_\phi} = \omega_\theta^2 + \omega_a^2 \tag{30}$$

where $$\omega_\theta^2 = \frac{K_\theta}{I_\theta}$$

and similarly, for precessional restraint:

$$\omega_A^2 = \omega_\phi^2 + \omega_a^2 \tag{31}$$

where $$\omega_\phi^2 = \frac{K_\phi}{I_\phi}$$

Thus, for either nutational or precessional restraint, the antiresonant frequency may be expressed as a function of gyro speed.

With elastic restraint about both θ and ϕ axes (undamped), the expression for the antiresonant frequency becomes:

$$\omega_A^2 = \left(\frac{\omega_\theta^2 + \omega_\phi^2 + \omega_a^2}{2}\right) \pm \left[\left(\frac{\omega_\theta^2 + \omega_\phi^2 + \omega_a^2}{2}\right) - \omega_\theta^2 \omega_\phi^2\right]^{1/2} \tag{32}$$

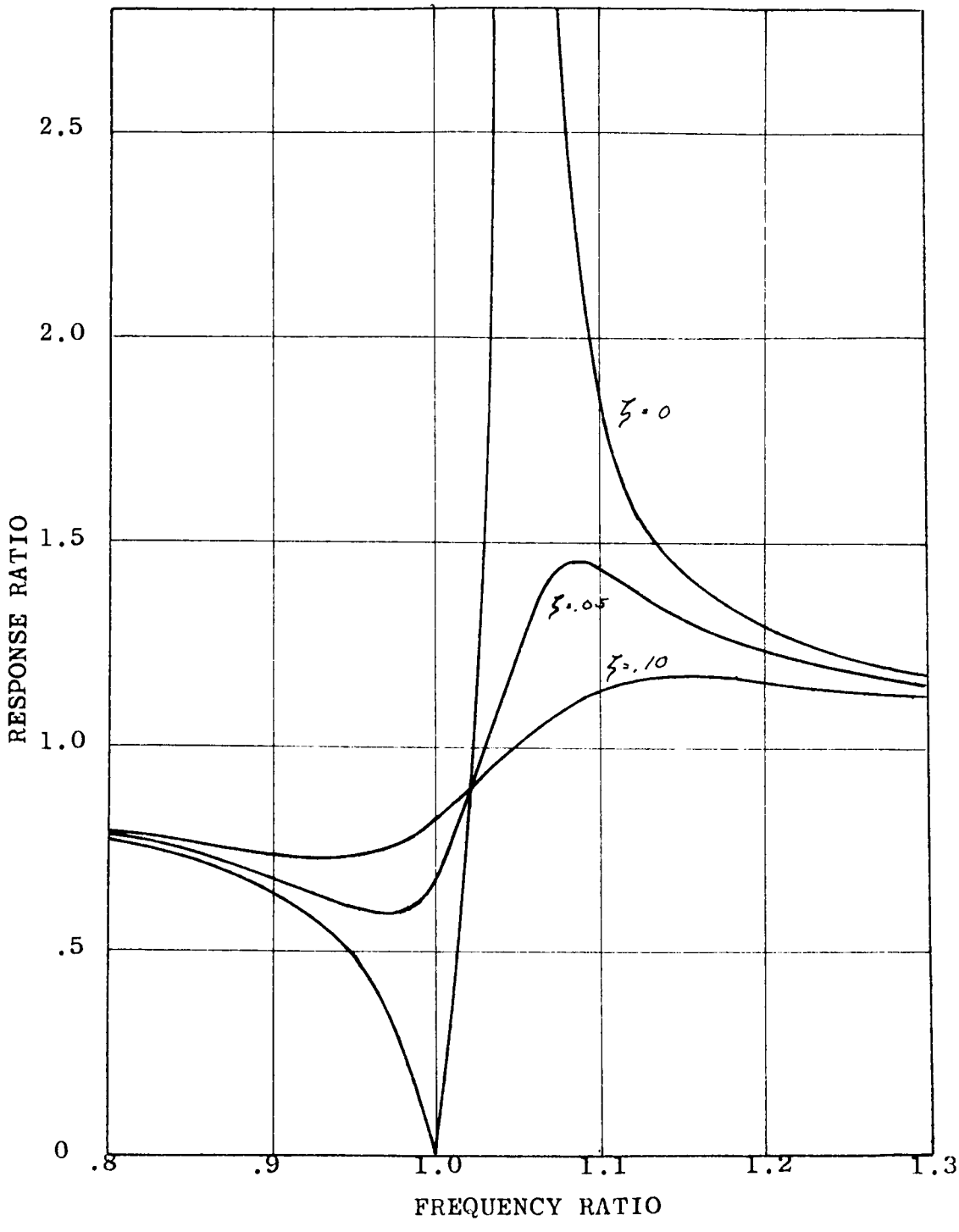

FIGURE 8.- RESPONSE RATIO VARIATION WITH FREQUENCY RATIO FOR A FRAHM ABSORBER

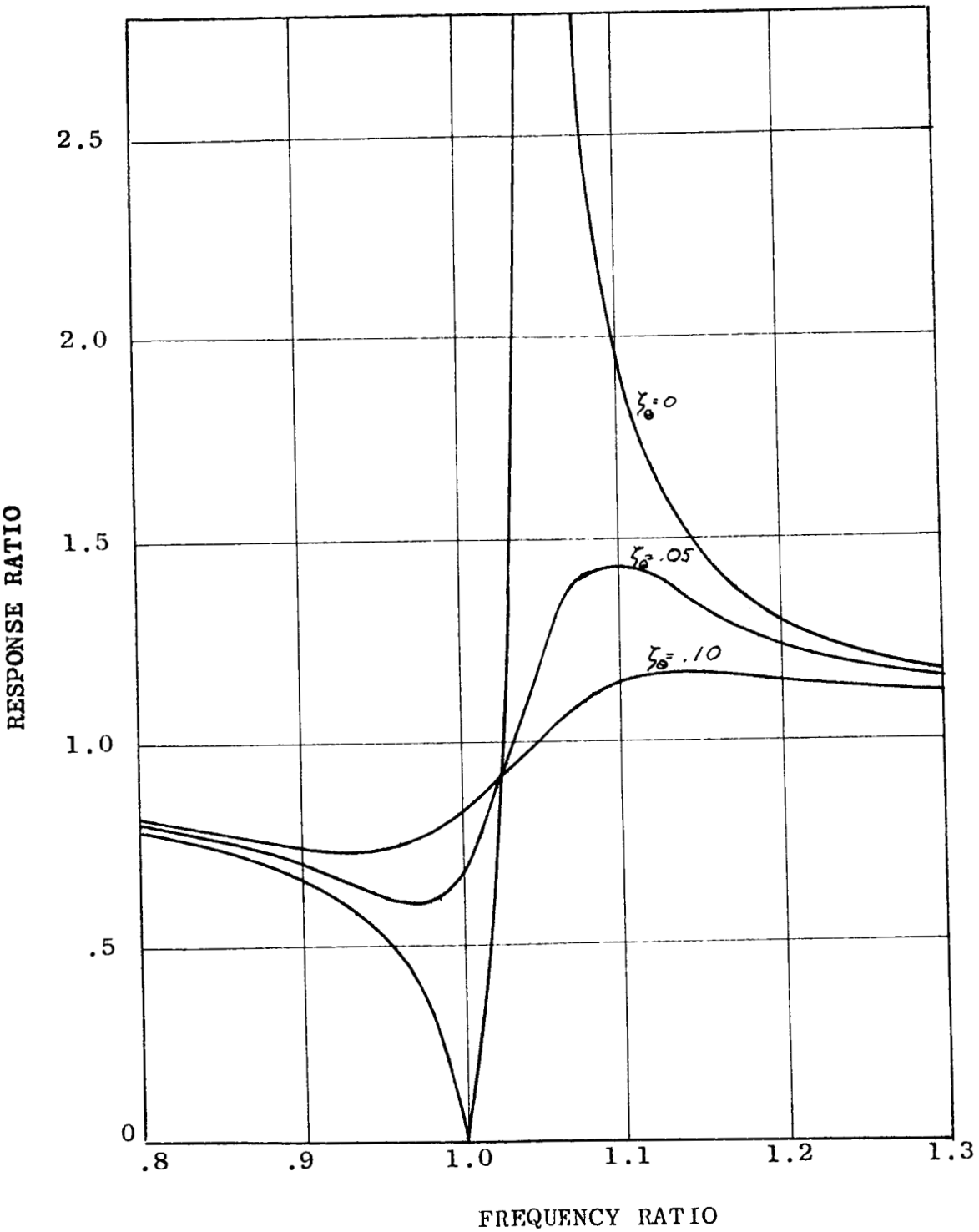

FIGURE 9.- RESPONSE RATIO VARIATION WITH FREQUENCY RATIO FOR A NUTATIONAL DAMPED GVA

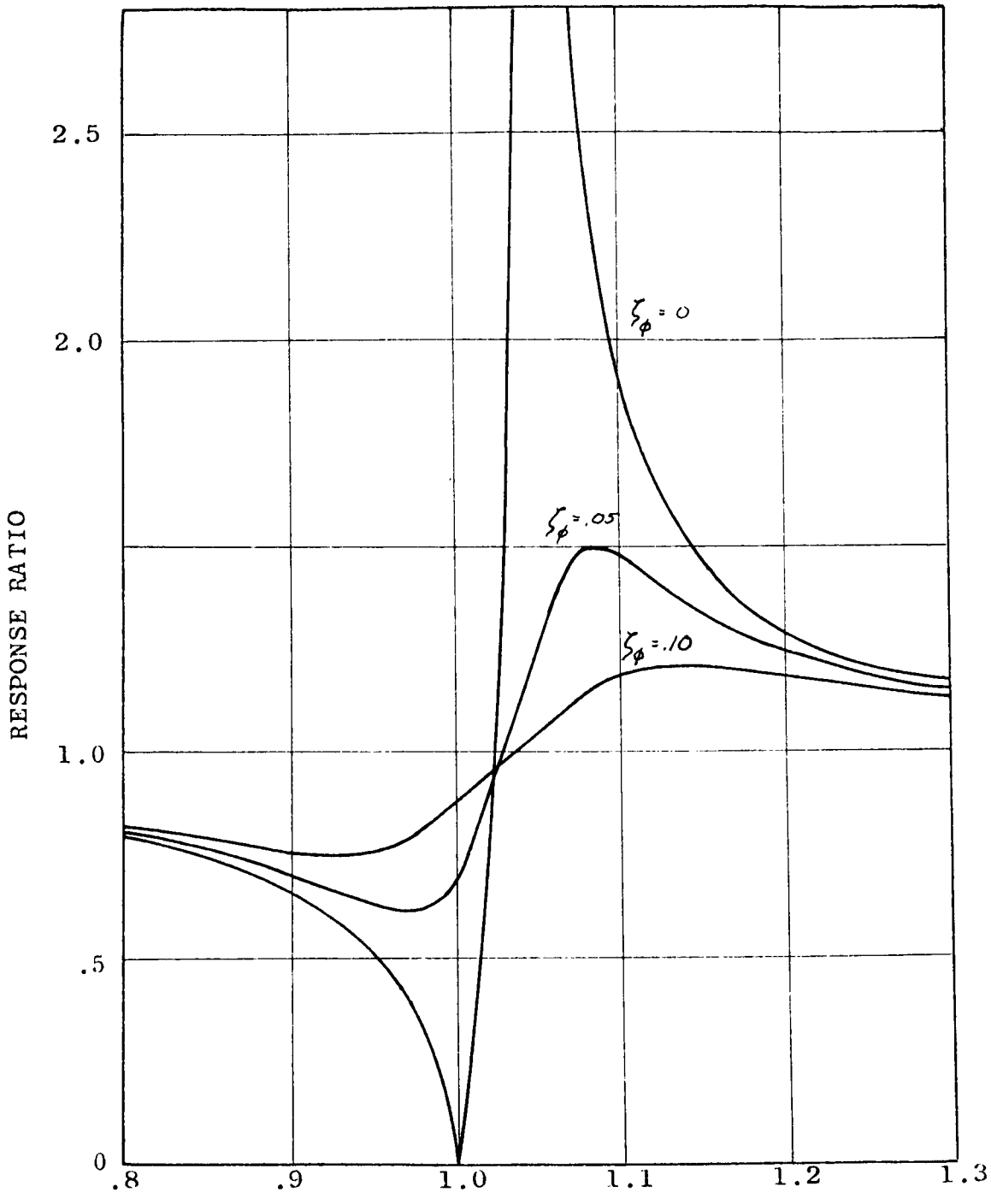

FIGURE 10.- RESPONSE RATIO VARIATION WITH FREQUENCY RATIO FOR A PRECESSIONAL DAMPED GVA

In plotting f_A as a function of gyro speed (Ω) for various values of ω_θ, ω_ϕ, and $\frac{I_z}{\sqrt{I_\theta I_\phi}}$, as in Figure 11, a family of curves are obtained which are asymptotic to the slope.

$$\frac{f_A}{\Omega} = \frac{I_z}{\sqrt{I_\theta I_\phi}} \tag{33}$$

and if $\omega_\theta = \omega_\phi$, the family of curves will also be symmetrical about $\omega_A = \omega_\theta = \omega_\phi$. Thus, there exists two antiresonant frequencies at a given gyro speed. The practicality of eliminating vibration at both frequencies may prove difficult in that the divergent slope characteristics of the antiresonant curves suggest "tuning" problems for minor excitation variances.

Structural Flexibility. - Excessive flexibility in those parts of the GVA structure designed to be rigid will cause the synchronization curve (see Figure 12) to be nonlinear. This phenomenon is essentially a variation in nutational resonance similar to the case discussed in Reference 4. This effect has been demonstrated experimentally in the GVA and should not be difficult to avoid by insuring, in the design of the GVA, that the first bending natural frequency of the "rigid" GVA structure is very high compared to the highest frequency of excitation.

Representing structural flexibility in the GVA by the spring hinge in the barrel in Figure 13, the equation for $\delta = 0$ becomes:

$$\begin{bmatrix} K_\alpha - \omega^2(I_{\theta'} + mb^2) & +iI_z\Omega\omega & -K_\alpha - \omega^2 mab \\ -iI_z\Omega\omega & -I_\phi\omega^2 & 0 \\ -\omega^2 ab m - K_\alpha & 0 & -\omega^2 a^2 m + K_\alpha \end{bmatrix} \begin{vmatrix} \theta \\ \phi \\ \alpha \end{vmatrix} = 0 \tag{34}$$

Equation (34) is a quadratic in ω^2 after dividing out the root $\omega^2 = 0$. If $K_\alpha = \infty$, the roots are:

$$\omega_a = 0 \quad , \omega_a = \frac{I_z\Omega}{\sqrt{I_\theta I_\phi}} \tag{35}$$

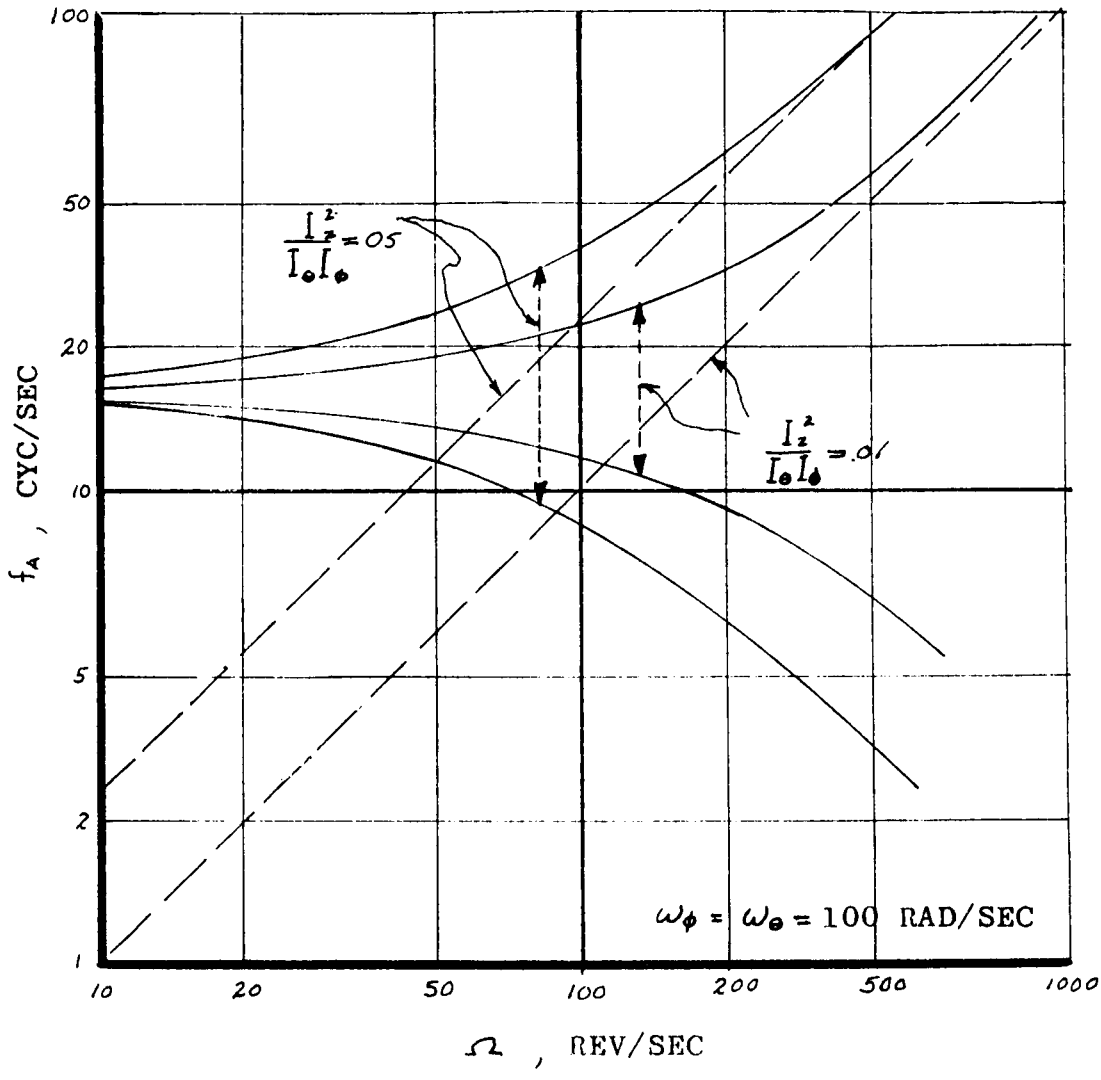

FIGURE 11.- EFFECT OF ELASTIC RESTRAINT ON THE ANTIRESONANT FREQUENCY

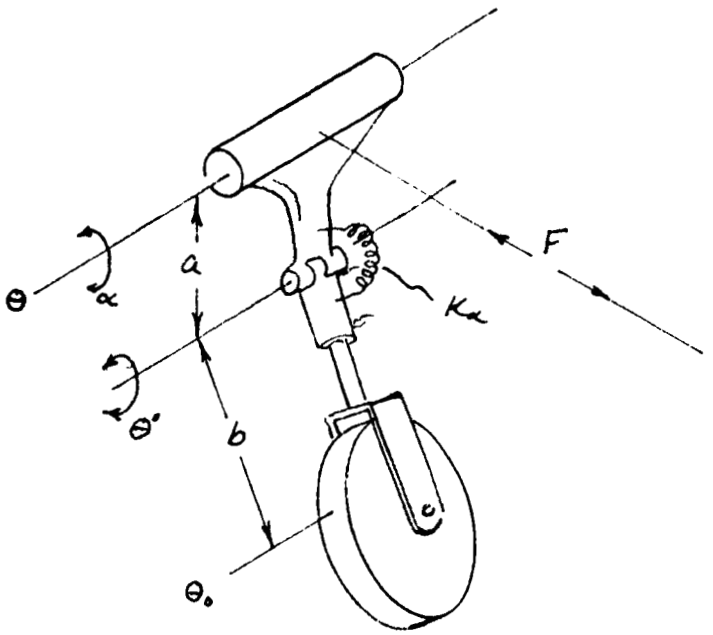

FIGURE 13.- REPRESENTATION OF STRUCTURAL FLEXIBILITY

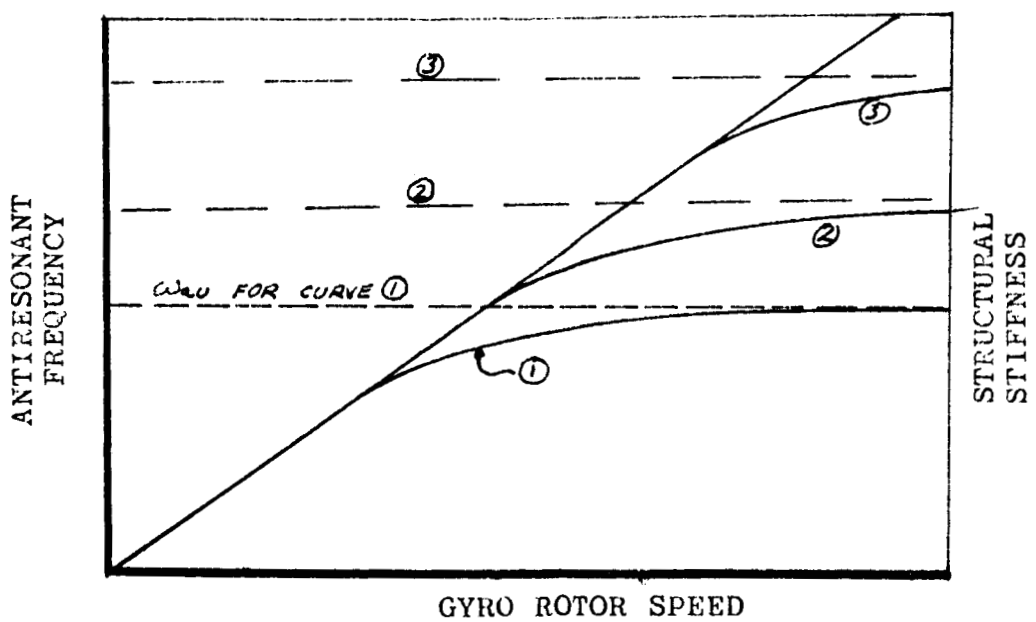

FIGURE 12.- EFFECT OF STRUCTURAL FLEXIBILITY ON THE ANTIRESONANT FREQUENCY

which is the case with rigid structure. When $\Omega = \infty$, the roots are:

$$\omega = 0 \quad , \quad \omega_{au}^2 = \frac{K_\alpha}{M_\beta^2} \tag{36}$$

where ω_{au} is the antiresonant frequency asymptote. When $\Omega = 0$, the roots are:

$$\omega = 0 \quad , \quad \omega_{al}^2 = \frac{I_\theta}{I_{\theta'}} \omega_{au}^2 \tag{37}$$

Noting, in Equation (37), that $I_\theta > I_{\theta'}$, it is evident that the first bending natural frequency will be greater than the asymptotic antiresonant frequency. However, the bending natural frequency should be close to the asymptotic antiresonance ($I_\theta \simeq I_{\theta'}$) for most GVA designs, allowing use of the natural frequency as an approximation of ω_{au}. If ω_{au} is very high, the synchronization is essentially linear in the lower frequency range.

Stability. - The dynamic stability of the GVA was investigated for the linearized equations of motion. The pertinent equation is that formed by the matrix on Page 15 and is a quartic of the form:

$$S^4 + A_3 S^3 + A_2 S^2 + A_1 S^1 + A_0 = 0 \tag{38}$$

For stability, the Routh criteria set forth, for instance, in Reference 1, requires that all coefficients (A_0, A_1, A_2, A_3) be positive, and

$$1 \geq \frac{A_1^2 + A_3 A_0}{A_1 A_2 A_3} \tag{39}$$

where: $A_0 = \omega_\theta^2 \omega_\phi^2 \Big/ \left(1 - \frac{S^2}{M_T I_\theta}\right)$

$$A_1 = \left[2\zeta_\phi \omega_\theta^2 + 2\zeta_\theta \omega_\phi^2\right] \Big/ \left(1 - \frac{S^2}{M_T I_\theta}\right)$$

$$A_2 = \left[\omega_\theta^2 + \omega_\phi^2 \left(1 - \frac{S^2}{M_T I_\theta}\right) + \omega_a^2 + 4\zeta_\theta \zeta_\phi\right] \Big/ \left(1 - \frac{S^2}{M_T I_\theta}\right)$$

$$A_3 = \left[2\zeta_\theta + 2\zeta_\phi \left(1 - \frac{S^2}{M_T I_\theta}\right)\right] \Big/ \left(1 - \frac{S^2}{M_T I_\theta}\right)$$

The above coefficients are always positive, since physical parameters of the GVA dictate that $S^2/M_T I_\theta$ is always less than one; therefore, the first criterion for stability is satisfied.

Since stability of the GVA, as a function of gyro speed, is of major interest, Equation (39) was re-arranged to determine its stability as a function of gyro speed or:

$$\omega_a^2 \geq \frac{\left(1 - \frac{S^2}{M_T I_\theta}\right)\left(2\zeta_\phi \omega_\theta^2 + 2\zeta_\theta \omega_\phi^2\right)^2 + \left[2\zeta_\theta + 2\zeta_\phi \left(1 - \frac{S^2}{M_T I_\theta}\right)\right]^2 \omega_\theta^2 \omega_\phi^2}{\left[2\zeta_\phi \omega_\theta^2 + 2\zeta_\theta \omega_\phi^2\right]\left[2\zeta_\theta + 2\zeta_\phi \left(1 - \frac{S^2}{M_T I_\theta}\right)\right]} - \omega_\theta^2 - \omega_\phi^2 \left(1 - \frac{S^2}{M_T I_\theta}\right) - 4\zeta_\theta \zeta_\phi \tag{40}$$

Substituting in the above expression $\zeta_\phi = 0$ gives the following results:

$$\omega_a^2 \geq 0 \tag{41}$$

also, substituting in $\omega_\phi^2 = 0$ (effective structural restraints) in Equation (40) gives:

$$\omega_a^2 \geq -\frac{\omega_\theta^2 \zeta_\theta + 4\zeta_\theta^2 \zeta_\phi + 4\zeta_\phi^2 \zeta_\theta \left(1 - \frac{S^2}{M_T I_\theta}\right)}{\zeta_\theta + \zeta_\phi \left(1 - \frac{S^2}{M_T I_\theta}\right)} \tag{42}$$

Substituting in $\zeta_\theta = 0$ and $\omega_\theta^2 = 0$ gives similar results.

It is seen from these results with zero damping or elastic restraints, that the GVA is stable over the complete RPM range of the gyro.

Discussion. - Nonlinear equations of the GVA type, three simultaneous unlinearized equations of motion having periodic coefficients, generally cannot be solved exactly. This type is usually linearized, or approximate solutions are obtained by perturbation technique, analog, etc. However, the GVA equations have been solved exactly for steady state periodic motion of the system. The solution is in the form of transcendental equations describing the response relation of angular amplitudes and forcing function amplitude and frequency.

As supplementary approaches to the solution of the GVA equations, a numerical solution, Runge-Kutta, was used to bear out a significant stability criterion,

$$SIN\ \Theta_1 = \left| \frac{F_o}{S\omega^2} + \frac{M_T \delta_1}{S} \right| \leq 1$$

derived in the analytic solution.

Analysis - Amplitude of θ. - Recalling that the GVA equations of motion can be written without the small angle restriction, and damping or spring terms:

$$I_\theta \ddot{\theta} + I_z \Omega \dot{\phi} (\cos \phi) + S (\cos \theta) \ddot{\delta} = 0 \tag{43}$$

$$I_\phi \ddot{\phi} - I_z \Omega \dot{\theta} (\cos \phi) = 0 \tag{44}$$

$$M_T \ddot{\delta} + S \frac{d}{dt} (\dot{\theta} \cos \theta) = F \tag{45}$$

Multiplying (43) by $\dot{\theta}$, (44) by $\dot{\phi}$, and substituting (45), there is obtained:

$$I_\theta \dot{\theta} \ddot{\theta} + I_\phi \dot{\phi} \ddot{\phi} - \frac{S^2}{2M_T} \frac{d}{dt} (\dot{\theta} \cos \theta)^2 = - \frac{S}{M_T} F \dot{\theta} \cos \theta \tag{46}$$

The left side of (46) is an exact derivative, and the solution is:

$$I_\theta (\dot{\theta}^2 - \dot{\theta}_o^2) + I_\phi (\dot{\phi}^2 - \dot{\phi}_o^2) - \frac{S^2}{M_T} \left[(\dot{\theta} \cos \theta)^2 - (\dot{\theta}_o \cos \theta_o)^2 \right]$$

$$= - \frac{2S}{M_T} \int_{t_o}^{t} F \dot{\theta} \cos \dot{\theta}\, dt \tag{47}$$

If the system is periodic to the extent that $\dot{\theta}$ and $\dot{\phi}$ return to initial values after time, t,

$$0 \equiv \int_{\tau_0}^{\tau_0+\tau} F\dot{\theta}(\cos\theta)\,d\tau = \int_{\tau_0}^{\tau_0+\tau} F\,d(\sin\theta) \rightarrow \int_{\tau_0}^{\tau_0+\tau} (\sin\theta)(\cos\omega\tau)\,d\tau = 0$$

$$\begin{cases} F = F_0 \sin\omega t \\ \text{and} \quad n\omega t = \tau \end{cases} \tag{48}$$

Integrating (45) directly yields:

$$M_T\dot{\delta} + S\,\overline{\sin\theta} = K_1 - \frac{F_0}{\omega}\cos\omega t \tag{49}$$

and again,

$$M_T\delta + S\sin\theta = -\frac{F_0}{\omega^2}\sin\omega t + K_1 t + K_0 \tag{50}$$

For periodic motion on δ_0, $K_1 = 0$, and the exact solution may be written:

$$M_T(\delta - \delta_0) + S(\sin\theta - \sin\theta_0) = -\frac{F_0}{\omega^2}\sin\omega t \tag{51}$$

or without loss of generality:

$$M_T\delta + S\sin\theta = -\frac{F_0}{\omega^2}\sin\omega t \tag{52}$$

$$M_T\dot{\delta} + S\,\overline{\sin\theta} = -\frac{F_0}{\omega}\cos\omega t \tag{53}$$

For periodic motion of the main mass, the displacement may be represented by a Fourier series as:

$$\delta = \sum (a_n \cos n\omega t + b_n \sin n\omega t) \tag{54}$$

substituting into (52) yields:

$$\sin\theta = -\frac{F_o}{S\omega^2}\sin\omega t - \frac{M_T}{S}\sum (a_n \cos n\omega t + b_n \sin n\omega t) \tag{55}$$

Rewriting (43) (using 53) yields:

$$I_\theta \dot\theta\ddot\theta + I_\phi \dot\phi\ddot\phi - M_T \dot\delta\ddot\delta = \frac{F_o}{\omega}(\cos\omega t)\ddot\delta \tag{56}$$

and by (54)

$$I_\theta \dot\theta\ddot\theta + I\dot\phi\ddot\phi - M_T\dot\delta\ddot\delta = -F_o\omega\cos\omega t\sum n^2(a_n\cos n\omega t + b_n\sin n\omega t) \tag{57}$$

Integration of (57) yields:

$$I_\theta(\dot\theta^2 - \dot\theta_o^2) + I_\phi(\dot\phi^2 - \dot\phi_o^2) - M_T(\dot\delta^2 - \dot\delta_o^2) = -2F_o\omega\int_{t=0}^{t=t}\cos\omega t\sum n^2(a_n\cos n\omega t + b_n\sin n\omega t)dt \tag{58}$$

For periodic motion, the left side vanishes at multiples of the period, hence:

$$0 = \int_{t=0}^{t=t}\sum a_n n^2(\cos\omega t)(\cos n\omega t)dt + \int_{t=0}^{t=t}\sum b_n n^2(\cos\omega t)(\sin n\omega t)dt \tag{59}$$

The second integral vanishes naturally for all values of n, while the first vanishes for all n except n = 1. Hence, a_1 must vanish as a necessary condition of periodicity. All remaining coefficients also vanish except for b_1, and the complete solution for (45) is:

$$\delta = \delta_1 \sin \omega t \tag{60}$$

and

$$\sin \theta = \sin \theta_1 \sin \omega t \tag{61}$$

where

$$\sin \theta_1 = -\left(\frac{F_0}{S\omega^2} + \frac{M_T \delta_1}{S} \right) \tag{62}$$

with the necessary condition:

$$\boxed{\left| \frac{F_0}{S\omega^2} + \frac{M_T \delta_1}{S} \right| \leq 1} \tag{63}$$

Analysis - Amplitude of ϕ. - Rewriting Equation (43):

$$\frac{d}{dt}(-\sin \phi) = \frac{I_e}{I_z \Omega} \ddot{\theta} + \frac{S}{I_z \Omega} (\cos \theta) \ddot{\delta} \tag{64}$$

and integrating using (60) and (61) yields:

$$\sin \phi = -\frac{I_e \omega (\sin \theta_1)(\cos \omega t)}{I_z \Omega (\cos \theta)} - \frac{S \omega \delta_1}{2 I_z \Omega}\left[(\cos \omega t)(\cos \theta) + \frac{\cos^2 \theta_1}{\sin \theta_1} \ln \left(\frac{(\sin \theta_1)(\cos \omega t) + \cos \theta}{\cos \theta_1} \right) \right] \tag{65}$$

where:

$$SIN\ \phi_1 = -\frac{I_\theta\,\omega\,(SIN\ \theta_1)}{I_z\,\Omega} - \frac{S\,\omega\,\delta_1}{2\,I_z\,\Omega}\left[1 + \frac{COS^2\theta_1}{SIN\ \theta_1}\,\ln\frac{1 + SIN\ \theta_1}{COS\ \theta_1}\right] \tag{66}$$

Integration of Equation (44) yields:

$$COS\ \phi = \left(\frac{\omega}{\omega_a}\right)\frac{\dfrac{COS^2\theta_1}{COS^2\theta} - \dfrac{S\,\delta_1\,(COS^2\theta)}{I_\theta\,(SIN\ \theta_1)}}{\sqrt{COS^2\theta_1 + \dfrac{S\,\delta_1\,(COS^2\theta)}{I_\theta\,(SIN\ \theta_1)}}} \tag{67}$$

The complete solution for the undamped, unrestrained GVA equations of motion is given by Equations (60), (61), (65), (66), and (67), with the stability criterion given by Equation (63).

Elastic Restraint and Damping. - When the effects of springs and damping are added to both the θ and ϕ axes of the GVA, then the solutions to the GVA exact equations of motion are:

$$SIN\ \theta = (SIN\ \theta_1)(SIN\ \omega t) \tag{68}$$

$$SIN\ \theta_1 = \left[\frac{M_T\,\delta_1}{S} + \frac{F_o}{\mu\,\omega^2}\right] \leqq 1.0 \tag{69}$$

$$\delta = \delta_1\ SIN\ \omega t \tag{70}$$

$$SIN\ \phi = +\frac{I_\theta\,\omega\,(SIN\ \theta_1)(COS\ \omega t)}{I_z\,\Omega\ COS\ \theta} + \frac{S\,\omega\,\delta_1}{I_z\,\Omega}\,(COS\ \omega t)(COS\ \theta)$$

$$-\frac{C\,(SIN\ \theta_1)(COS\ \omega t)}{2\,\omega\,I_z\,\Omega} + \frac{C_\theta\,\theta}{I_z\,\Omega} + \left[\frac{S\,\omega\,\delta_1\,(COS^2\theta_1)}{2\,I_z\,\Omega\,(SIN\ \theta)}\right.$$

$$\left.-\frac{b}{2\,\omega\,I_z\,\Omega}\right]\ln\left(\frac{(SIN\ \theta_1)(COS\ \omega t) + COS\ \theta}{COS\ \theta_1}\right) \tag{71}$$

$$\frac{I_\phi}{2}\left(\dot{\phi}^2_{\frac{\pi}{2}} - \dot{\phi}^2_o\right) + (\alpha_\theta + \alpha_\phi) + \frac{K_\phi}{2}\left(\phi^2_{\frac{\pi}{2}} - \phi^2_o\right) - \frac{I_\theta \omega^2 \sin^2\theta_1}{2}$$

$$- \frac{S\omega^2 \delta_1 (\sin\theta_1}{2} + (b+c)\sin\theta_1 = 0 \qquad (72)$$

where c and b are defined by:

$$K_\theta = \frac{b \tan\theta + c \sin\theta}{2\theta} = b + c \qquad (73)$$

and is an approximation for the spring constant on the θ axis, and where:

$$\alpha_\phi + \alpha_\theta = \int_o^{\frac{\pi}{2}} (C_\phi \dot{\phi}^2 + C_\theta \dot{\theta}^2)\, dt \qquad (74)$$

$$\dot{\phi} = \frac{-\left[\frac{I_\theta \omega^2 (\sin\theta_1)}{I_z \Omega(\cos\theta_1)} + \frac{S\omega^2 \delta_1 (\cos\theta_1)}{I_z \Omega}\right] + \frac{b \sin\theta_1}{2\cos\theta_1} + \frac{c \sin\theta_1}{2}}{\pm \sqrt{1 - \left(\frac{C_\theta \theta_1}{I_z \Omega}\right)^2}} \qquad (75)$$

$$\dot{\phi}_o = \frac{+\frac{C_\theta \omega a}{I_z \Omega}}{\sqrt{1 - \sin^2\phi_o}} \qquad (76)$$

$$\phi_{\frac{\pi}{2}} = \sin^{-1}\frac{C_\theta \theta_1}{I_z \Omega} \qquad (77)$$

$$\phi_o = \sin^{-1}(\sin\phi_o) \quad (at \quad t = 0) \qquad (78)$$

Considerable simplification results when $C_\theta = C_\phi = 0$, i.e.,

$$\frac{I_\phi \left(\dot{\phi}_{\frac{\pi}{2}}\right)^2}{2} - \frac{K_\phi \phi_o^2}{2} - \frac{I_\theta \omega^2 (\sin^2 \theta_1)}{2} - \frac{S \omega^2 \delta_1 (\sin \theta_1)}{2} + (b+c)(\sin \theta_1) = 0 \quad (79)$$

where:

$$\dot{\phi}_{\frac{\pi}{2}} = -\frac{I_\theta \omega^2 (\sin \theta_1)}{I_z \Omega \cos \theta_1} - \frac{S \omega^2 \delta_1 (\cos \theta_1)}{I_z \Omega} - \frac{b (\sin \theta_1)}{2 (\cos \theta_1)} + \frac{c (\sin \theta_1)}{2} \quad (80)$$

EXPERIMENTAL INVESTIGATION

Discussion

Tests of experimental working models of the Gyroscopic Vibration Absorber (GVA) have demonstrated feasibility and corroborated analysis of the discrete frequency absorber as reported in Reference 5. Analytical investigation of the effect of flexibility in the GVA structure was confirmed experimentally.

The test program described herein was designed to provide experimental proof of the two fundamental GVA principles, predicted by theory, which are necessary and sufficient to the establishment of feasibility of the GVA:

(a) A purely inertial gyroscopic system will produce an antiresonance of the mass to which it is attached (i.e. that such a system has a natural frequency when decoupled).

(b) The antiresonant frequency is proportional to the angular speed of the gyro.

To achieve these objectives, two experimental working models of the GVA were constructed and tested on an MB 50-pound shaker.

Experimental Model I

A preliminary GVA test model (Figure 14) was constructed using a scrap ball bearing driven by air jets, directed against the balls, and supplied by hanger pneumatic lines through a regulator. The bearing was free to precess about a diametral axis of the disc and to nutate about an axis roughly parallel to the gyro disc plane and displaced 9 1/2 inches from the disc center, as shown in Figure 15.

The model was attached to an MB C-11 shaker. A velocity transducer was clamped to the shaker armature and its output fed to an MB vibration meter.

The speed of the bearing was found to be very sensitive to the friction load, resulting from axial loading of the balls by the gyroscopic moment. While this turbine arrangement was capable of producing enormous bearing angular velocities, it provided very little torque at high speed. As a consequence of the low torque and apparently negative torque-speed curve, it was impossible to achieve a steady state antiresonant condition.

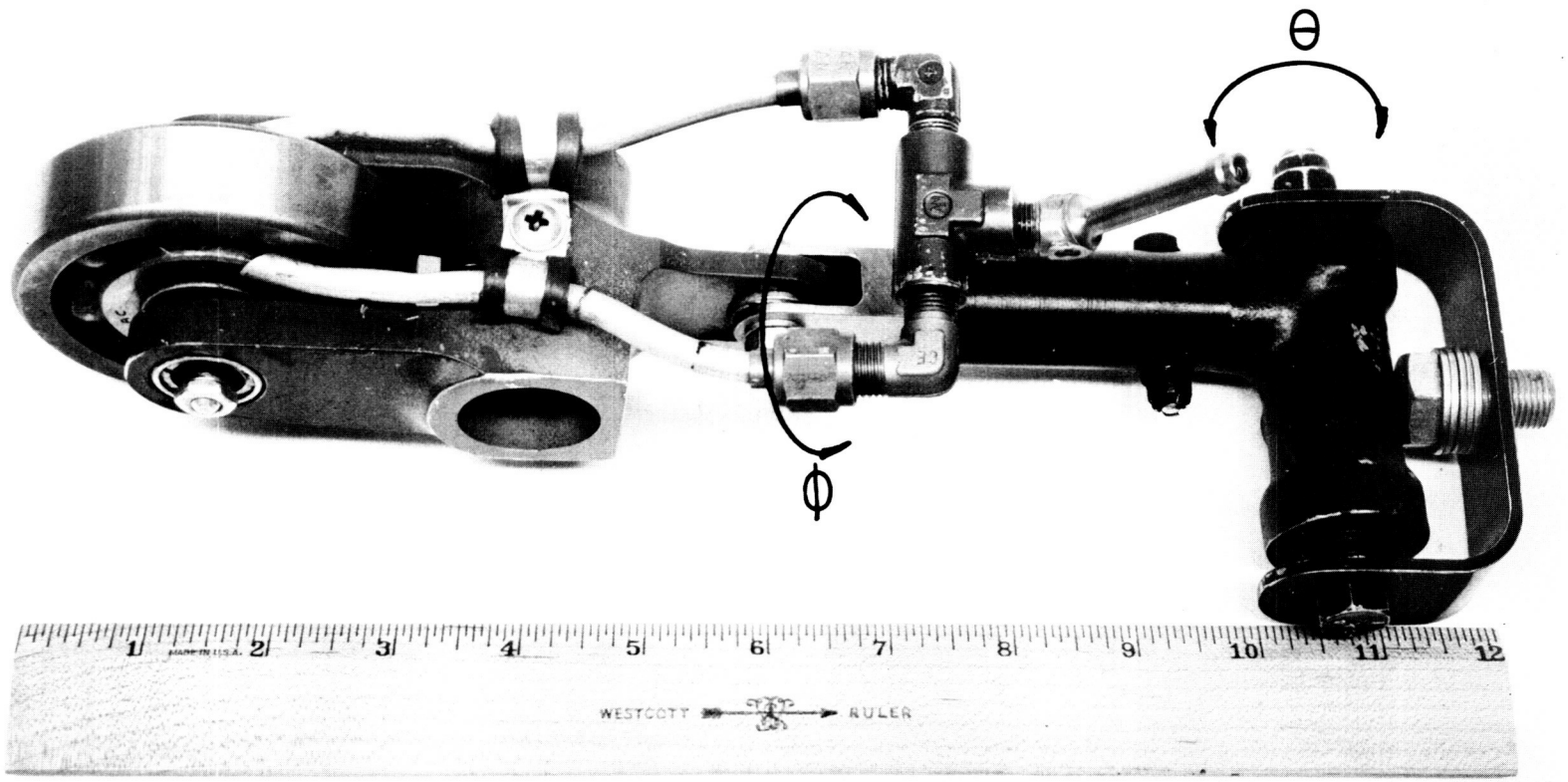

Figure 14. Preliminary GVA Test Model

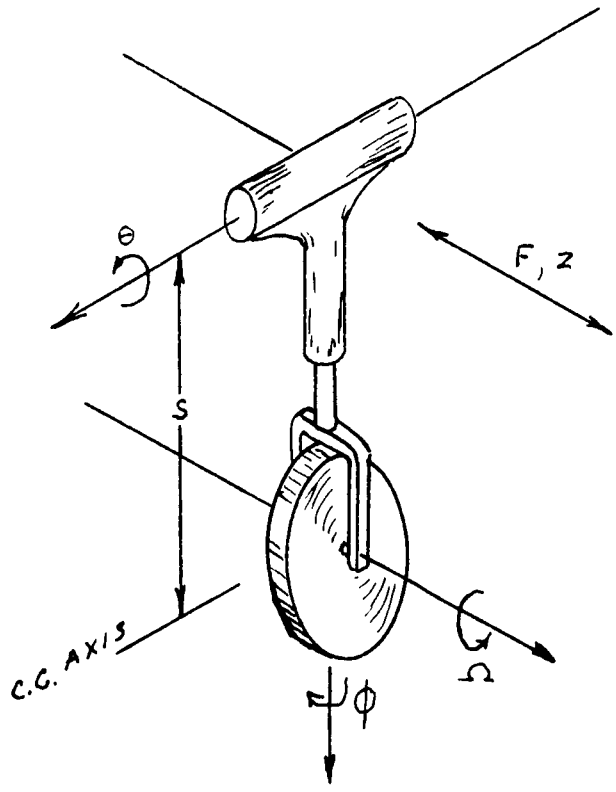

FIGURE 15.- DIAGRAM OF A GVA TEST MODEL

The transient antiresonant condition, with the gyro speed dropping, showed very pronounced attenuation, and the effect was repeatable. With the shaker operating, the gyro disc was manually positioned in a plane normal to the nutational axis which unloaded the rotor and allowed the gyro to accelerate. When the gyro (bearing) reached high speed, the gyro was turned manually about the ϕ axis (Figure 15) until it was in the plane of the θ axis and then released. The gyroscopic moments building up on the bearing caused the speed to decrease, and it would pass through the antiresonant gyro speed. At that speed, the armature pick-up output dropped by an order of magnitude, and the model executed the modes predicted in Reference 6.

This test provided qualitative confirmation of GVA theory, as discussed in Reference 6.

Experimental Model II

Description. - An experimental model of the Gyroscopic Vibration Absorber (Figure 16) was constructed by suitably mounting a standard Minneapolis-Honeywell JG-7005 rate gyro so that the assembly has the type of GVA mechanical action described in Reference 6.

The rate gyro was left entirely intact and mounted in the as-supplied condition (complete with rubber mounting pads bonded to gyro base) to the vertical face of an aluminum angle. Two rod end bearings with female threads were attached to the horizontal face of the angle by screws. While this arrangement has circuitous load paths and allows much greater flexure than normal design arrangements, it seemed sufficiently representative of a GVA design for demonstration and experimentation purposes. An alternative design that is contemplated for the future is shown in Figure 17.

The rate gyro is equipped with removable spring restraint about the ϕ axis (Figure 16). The spring rate about axis ϕ was found to be 3.59 inch-pounds/radian by force-deflection measurements. The static natural frequency of the gyro about the precessional (ϕ) axis was measured as 8.0 c.p.s., by plucking the gyro and recording the rudder-control circuit breaker blips (with a D.C. signal) on an oscillograph. With known static natural frequency and rotational spring rate, the inertia in precession (ϕ) was calculated at .549 pound-inches squared.

The manufacturer lists the momentum ($I_z \Omega$) of the rate gyro as 3.0×10^6 gm-cm^2/second (1.023×10^3 pound-inch^2/second) at 24,000 RPM which gives $I_z = .4075$ pound-inches^2.

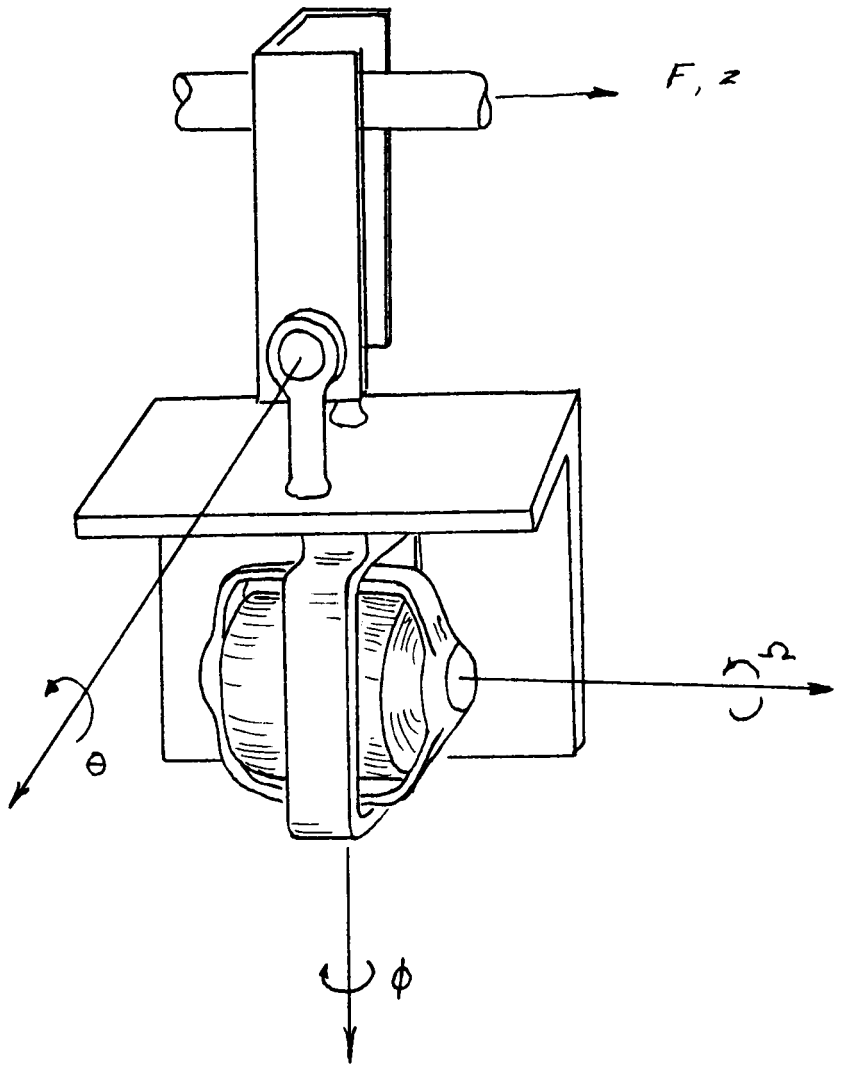

FIGURE 16.- SCHEMATIC OF THE GVA

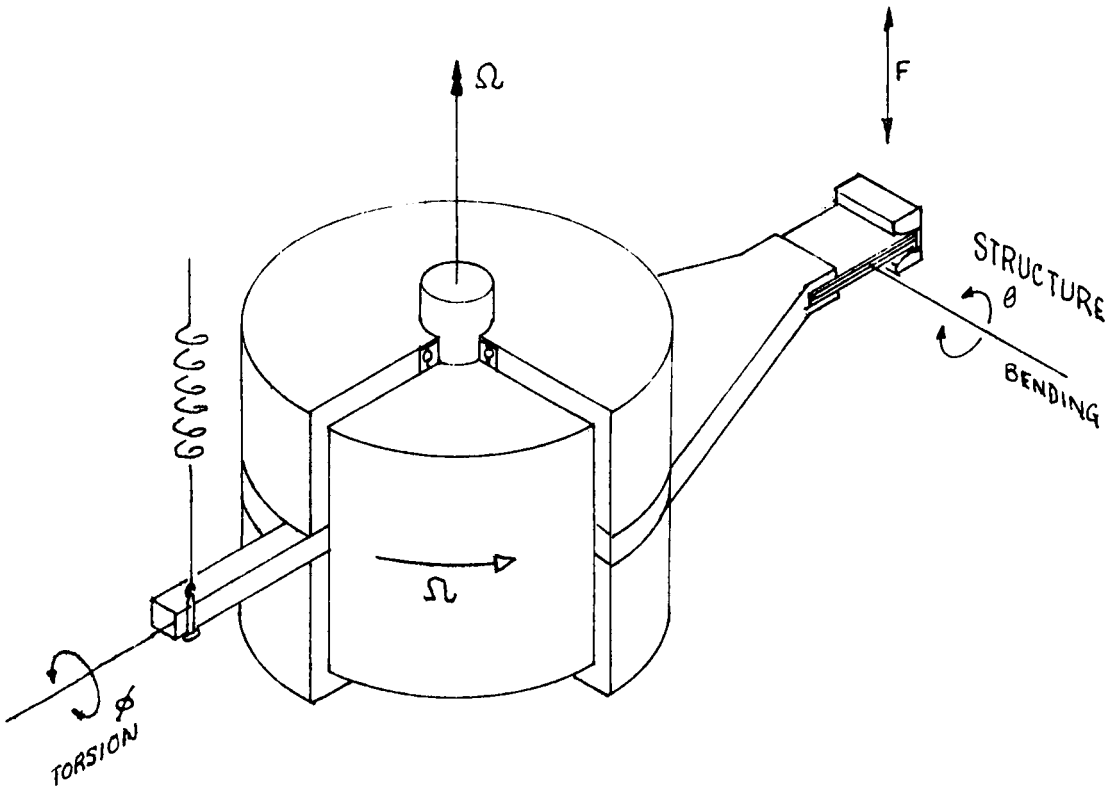

FIGURE 17.- AN ALTERNATE GVA CONFIGURATION

To obtain the nutational inertia (I_θ), the pendular period of the GVA model was clocked and found to be 0.625 seconds. The location of the center of gravity was found by accurately weighing the model and by using a scale as one reaction in a simple-beam support of the model. Treating the GVA as a compound pendulum oscillating about the θ axis, the nutational inertia was obtained:

$$I_\theta = \frac{t^2 \ell W}{4\pi^2} = 37.7 \text{ pound-inches}^2$$

Summary of the Physical Parameters of the GVA Experimental Model II:

ω_ϕ	=	8.0 c.p.s.	I_z	=	.4075 lbs-in^2
K_ϕ	=	3.59 in-lbs/rad	I_θ	=	37.7 lbs-in^2
I_ϕ	=	.549 lbs-in^2	ℓ	=	3.58 inches
			W	=	2.75 pounds

Instrumentation. - The GVA model was mounted to an MB Type C-11 Electromagnetic Shaker as shown in Figure 18. An MB velocity pickup was clamped to a flange on the shaker armature and the pickup output fed to an MB vibration meter.

An electronic counter was hooked in parallel with the rate gyro synchronous motor terminals so that the counter read line frequency (400 c.p.s.) with the power on and gyro speed (generated emf pulse count) with motor power off. The deceleration rate is so low, 260 seconds to go from 420 RPS to 60 RPS (see Figure 19), that sufficient speed resolution could be obtained at the antiresonance during gyro "run-down" using the electronic counter; this scheme eliminated the need for inverters and associated equipment.

Gyro speed, as measured by the electronic counter, was cross-checked against stroboscope measurement of speed. The stroboscope was calibrated against reed vibration at line frequency. The stroboscope range did not extend to 400 RPS, so it was used to measure the second, third, fourth, and fifth subharmonics of gyro speed.

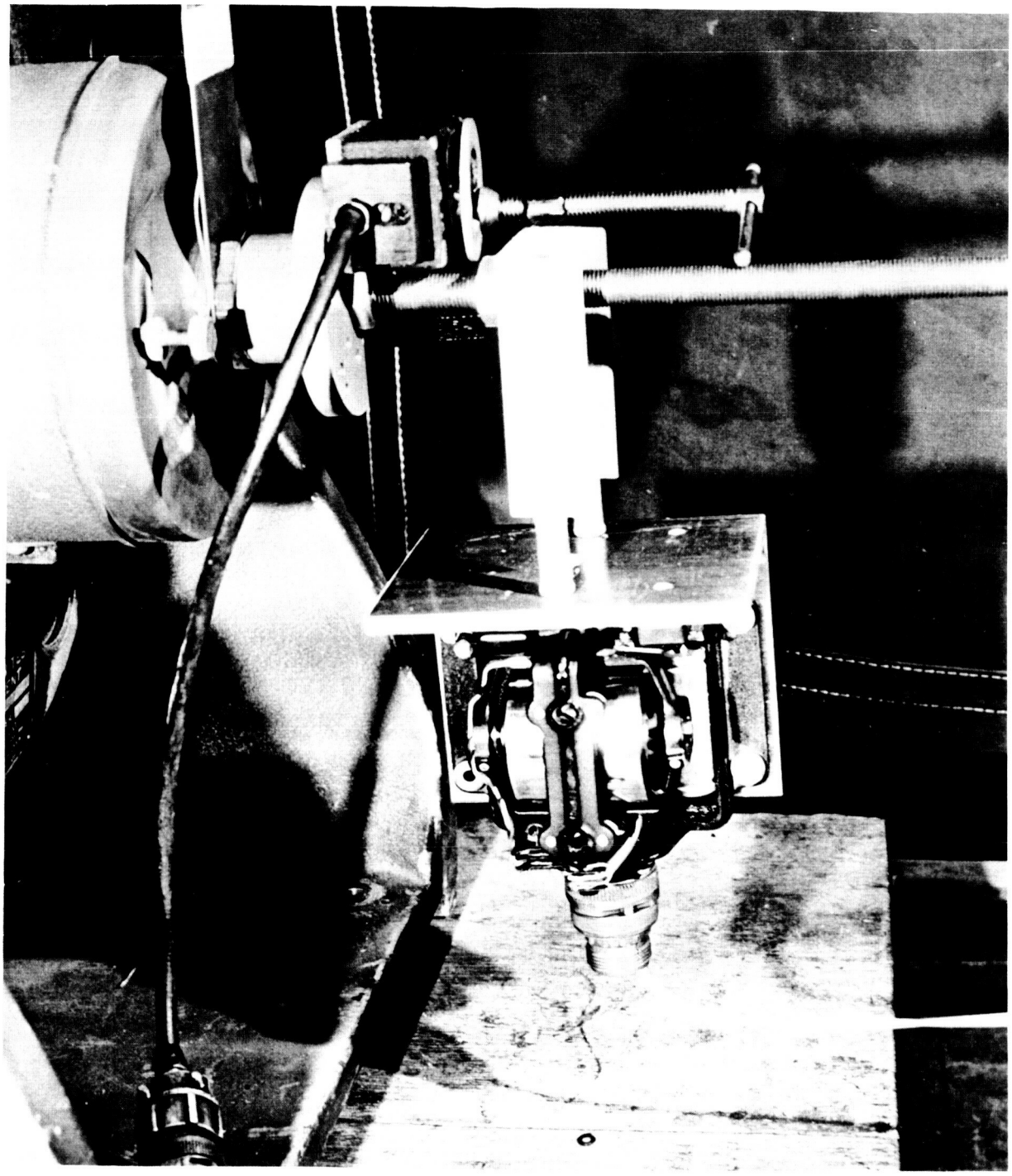

Figure 18. Second GVA Test Model

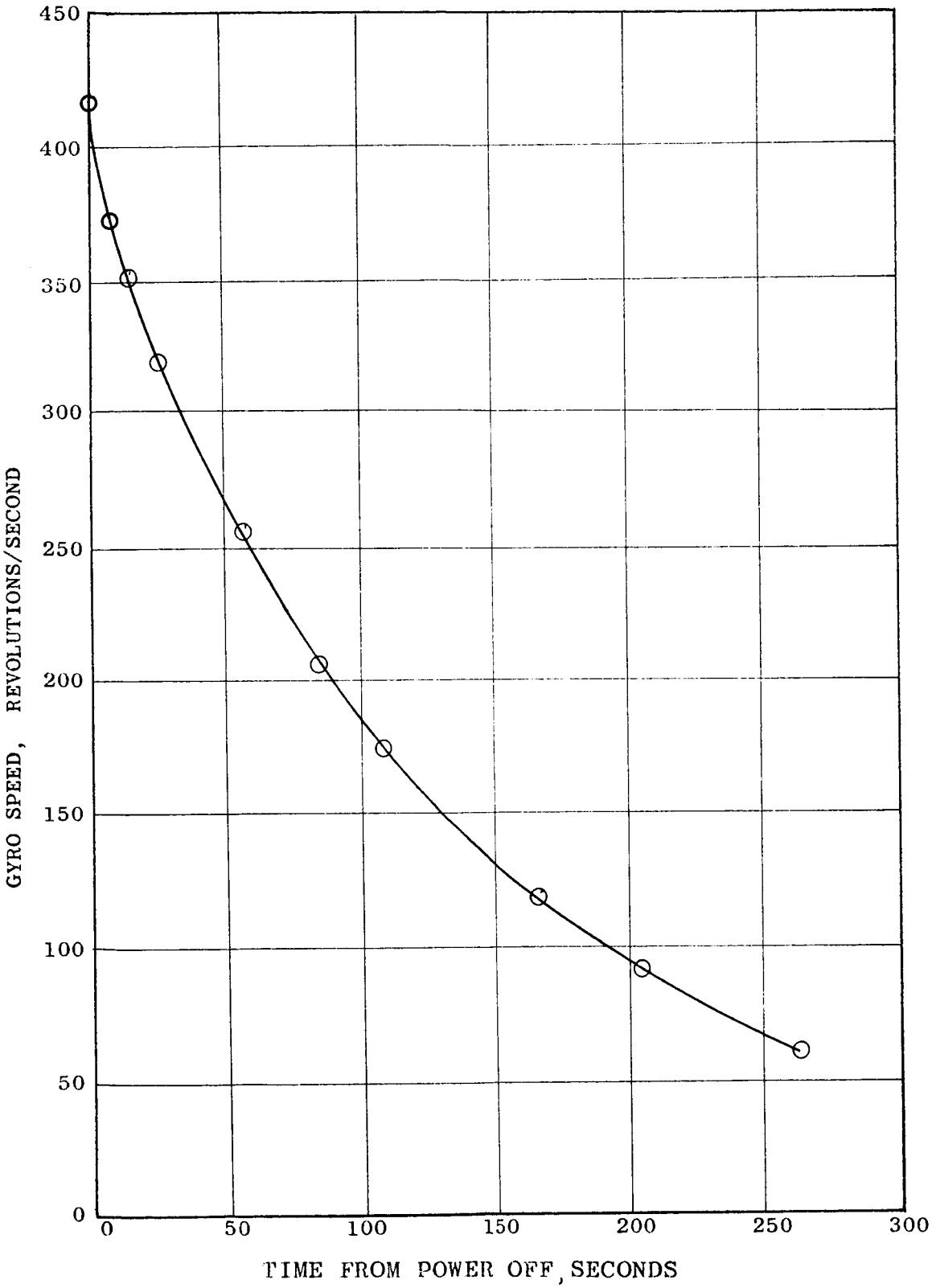

FIGURE 19.- GVA TEST MODEL DECELERATION RECORD

Increased resolution of the shaker armature ammeter was obtained by connecting a Ballantine peak-to-peak VTVM to the oscilloscope terminals of the MB control console. It was found that there is a 10:1 relationship between the voltage across the CRO terminals and the armature current throughout the range of excitation frequency used in the tests.

Discussion - Model II. - With the gyroscope motor not turning and with a constant .22 amps on the shaker armature, the armature vibratory velocity was measured at steady-state excitation frequencies ranging from 10 c.p.s. to 100 c.p.s., yielding the upper curve shown in Figure 20. Under the same conditions, except that the gyro was turning at 380 revolutions/second, the antiresonant curve was obtained. Note that 98.3 per cent of the vibration was eliminated at the antiresonance. The very broad bandwidth in this case is a result of the high absorber mass to armature mass ratio, and is not relevant to the GVA concept as such. The bandwidth of an undamped linear GVA, operating through small angles, should be slightly smaller than the bandwidth of a Frahm absorber of the same absorber mass to main mass ratio.

The peak velocity in resonance was not measured in gathering the data shown in Figure 20. To avoid damage to the delicate instrument bearings in the rate gyro, the resonant frequency was passed through quickly.

It was found that operation at .50 amperes on the shaker caused such excessive deflection in the gyro gimbal structure that the upper gyro bearing on the precessional (ϕ) axis would jump its socket and jam after about three minutes running time. Rather than mutilating the rate gyro by structural stiffening of the casting to correct this problem, the shaker armature amperage was reduced to .22 amps. This necessitated use of a VTVM on the console oscilloscope output to increase effective ammeter resolution. No further bearing difficulties were encountered with the reduced amperage.

To determine the variation in antiresonant frequency with gyro speed, the excitation frequency was set lower than the antiresonant frequency with top gyro speed (420 revolutions/second). The gyro motor was then turned off and the gyro allowed to decelerate while its speed was monitored on the Electronic Counter. As the gyro reached a speed which made the excitation frequency an antiresonant frequency, the vibration meter would register a null. The Electronic Counter reading of gyro speed at the null was recorded. Figure 21 shows a plot of antiresonant frequency versus gyro speed from test, and a plot of the values predicted from Equation (31). The test points begin to differ significantly from theory at about 15 c.p.s.

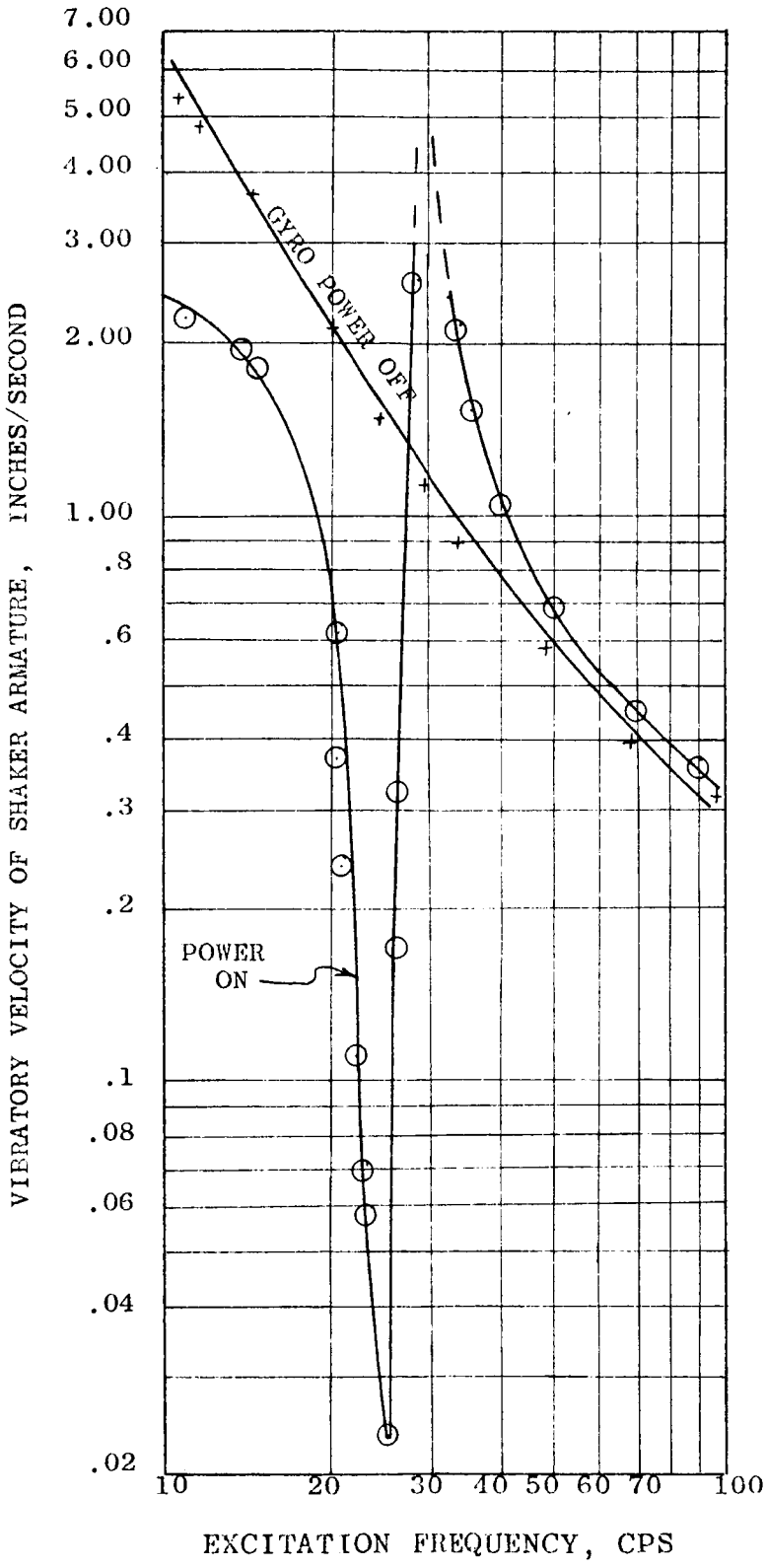

FIGURE 20.- VARIATION OF VELOCITY RESPONSE WITH FREQUENCY

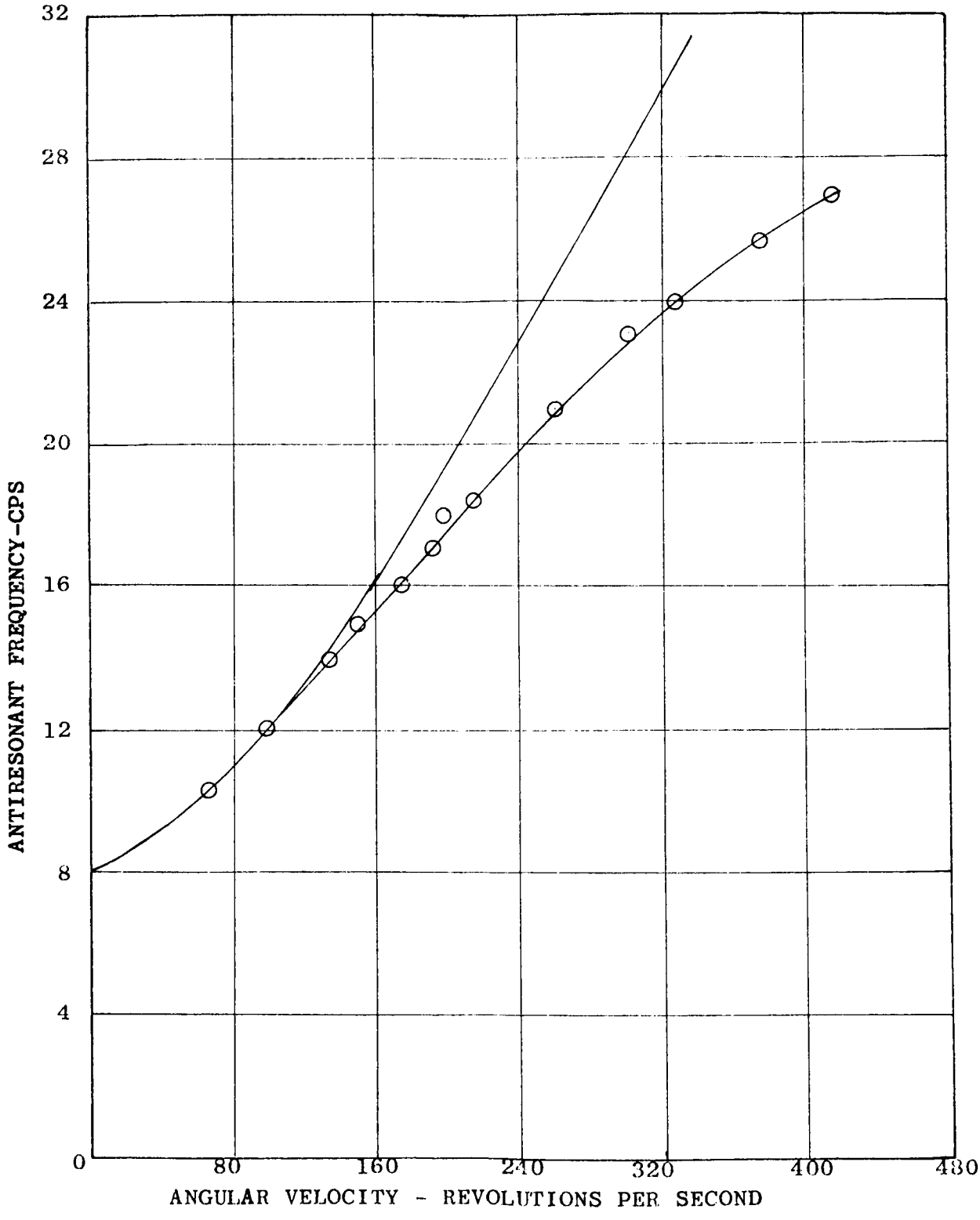

FIGURE 21.- VARIATION OF ANTIRESONANT FREQUENCY WITH GYRO ROTOR SPEED

The ϕ springs were removed from the gyro and the points (shown as ⊙) in Figure 22 were obtained. At $\omega >$ 14 c.p.s., these test points differ significantly from the prediction of Equation (15). It was suspected that the discrepancy between theory and test was a consequence of excessive structural flexibility, inherent in the model, from the rubber mounts on the gyro base, thin gimbal structure, etc. An analysis was performed on the system, shown in Figure 13, to determine theoretically effect of structural flexibility. As shown by Equation (36), flexibility of the type described in Figure 13 would cause the antiresonant frequency to asymptotically approach $\sqrt{\frac{K}{ma^2}}$ as the gyro speed Ω approaches infinity. At $\Omega = 0$, there are two antiresonant frequencies (Equation 37): $\omega = 0$ and $\omega = \sqrt{\frac{I_\theta}{I_{\theta'}}}\,\omega_{au}$. Although Figure 13 describes an arrangement which can hardly be regarded as a precise representation of the actual model flexibilities, and although $I_{\theta'}$ is not precisely known for the complex model structure, it was felt that the resulting Equation (36) should be sufficient to approximately predict model performance. It was reasonable to assume that $\frac{I_\theta}{I_{\theta'_o}} \approx \frac{I_\theta}{I_{\theta_o}}$ and that 28 c.p.s. $< \omega_{au} <$ 50 c.p.s. for the upper (⊙) experimental points in Figure 22. Equation (37) then predicted that an antiresonant frequency on the shaker armature at zero gyro speed would be found between 106.5 c.p.s. and 190 c.p.s., if structural flexibility was the cause of the nonlinear antiresonance curve. After this analytical prediction was derived, the model was shaken at $\Omega = 0$, and a very distinct armature antiresonance was found at 170 c.p.s. Another antiresonance was found above 400 c.p.s., showing that the model has several additional degrees of freedom beyond the ideal design configuration.

An additional proof that the nonlinear curve resulted from model deficiencies rather than inherent limitations of the GVA, the system was "softened" by placing two rubber grommets in series between the shaker armature stud and the aluminum channel adapter. As predicted, the asymptotic antiresonant frequency was lowered (see Figure 22, △ curve). The system was then "softened" further in the same manner, and, as expected, the asymptotic antiresonant frequency dropped further (Figure 22, ⊡ curve).

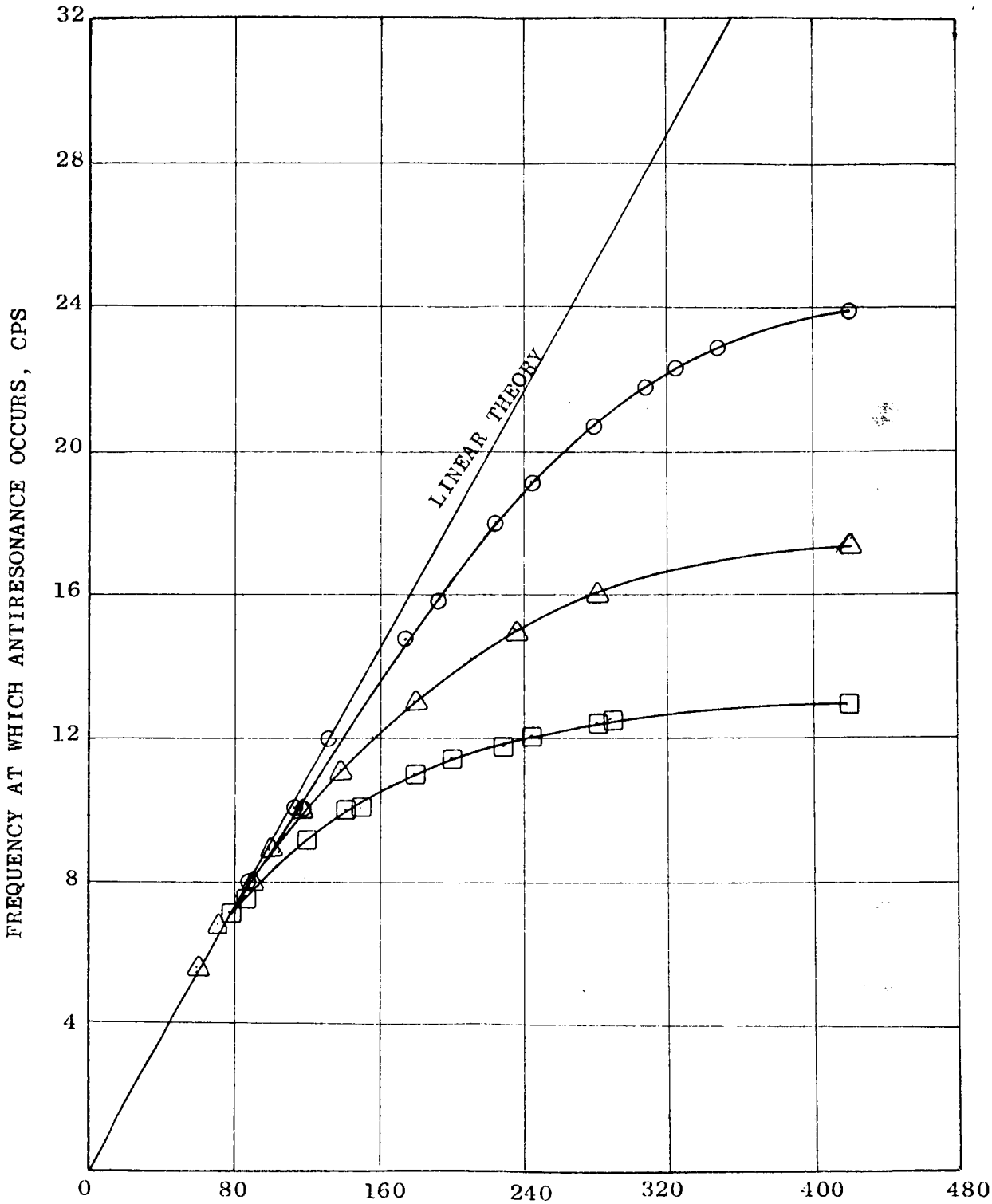

FIGURE 22.- EFFECT OF STRUCTURAL FLEXIBILITY ON ANTIRESONANT FREQUENCY

From these results, it is reasonable to conclude that the theory of the GVA accurately describes the operation of the GVA under the assumed conditions of rigid structure and small angles. It is evident that ordinary design practices would provide sufficient structural rigidity to maintain a linear variation of ω_a with Ω up to very high frequencies.

The angular speed of the gyro is plotted against the time elapsed from power cutoff in Figure 19. Two exponential curves ($\Omega = 420\ e^{-1.487 \times 10^{-2}t}$ and $\Omega = 420\ e^{-1.02 \times 10^{-2}t}$), with slopes which appeared to bracket the test data slope at 420 RPS, were fitted to the data. Differentiation of these equations at $t = 0$ yielded the deceleration at $\Omega = 420$ RPS. Because the motor torque is just sufficient to overcome the torque due to friction, air resistance, etc. at steady-state speed, the instantaneous deceleration at $t = 0$ times the gyro inertia, I_z, should equal the motor torque. With the gyro under vibratory excitation at antiresonance, the deceleration curve obtained is identical to the unexcited case, showing that power consumption in the model motor is independent of the GVA vibratory load.

Calculations show that the instantaneous torque at power cutoff ($t = 0$, 420 RPS) is between .0284 inch-pounds and .0414 inch-pounds; the power output of the synchronous motor is, therefore, between .01139 horsepower and .0166 horsepower.

OTHER CONFIGURATIONS

Parallel GVA Mounting

Analysis. - Consideration was given to the mounting of two identical GVA's with the same rotor speed, one damped and one undamped, as in Figure 23, with the expectation of obtaining a zero response ratio at the antiresonant frequency and a damped response at the resonant frequency. This was realized. The analysis leading to this result was similar to that presented on Page 14 , "Small Angular Motion". The linearized equations of motion are as follows, where subscript 1 or 2 indicate which GVA is considered:

$$
\begin{aligned}
I_{\theta_1}\ddot{\Theta}_1 + I_{z_1}\Omega\dot{\phi}_1 + S_1\ddot{\delta} &= 0 \\
I_{\theta_2}\ddot{\Theta}_2 + I_{z_2}\Omega\dot{\phi}_2 + S_2\ddot{\delta} + C_{\theta_2}\dot{\Theta}_2 &= 0 \\
I_{\phi_1}\ddot{\phi}_1 - I_{z_1}\Omega\dot{\Theta}_1 &= 0 \\
I_{\phi_2}\ddot{\phi}_2 - I_{z_2}\Omega\dot{\Theta}_2 + C_{\phi_2}\dot{\phi}_2 &= 0 \\
M_T\ddot{\delta}_1 + S_1\ddot{\Theta}_1 + S_2\ddot{\Theta}_2 &= F
\end{aligned}
\qquad (81)
$$

As before, a steady-state solution of the form, $q = Qe^{iwt}$, is assumed, and the matrix form is:

$$
\left[\begin{array}{c|c|c|c|c}
-S_1\omega^2 & -I_{\theta_1}\omega^2 & 0 & i I_{z_1}\Omega\omega & 0 \\
\hline
-S_2\omega^2 & 0 & -I_{\theta_2}\omega^2 + i\omega C_\theta & 0 & i I_{z_2}\Omega\omega \\
\hline
0 & -i I_{z_1}\Omega\omega & 0 & -I_{\phi_1}\omega^2 & 0 \\
\hline
0 & 0 & -i I_{z_2}\Omega\omega & 0 & -I_{\phi_2}\omega^2 + i\omega C_\phi \\
\hline
-M_T\omega^2 & -S_1\omega^2 & -S_2\omega^2 & 0 & 0
\end{array}\right]
\left[\begin{array}{c} \delta \\ \theta_1 \\ \theta_2 \\ \phi_1 \\ \phi_2 \end{array}\right]
=
\left[\begin{array}{c} 0 \\ 0 \\ 0 \\ 0 \\ F \end{array}\right]
$$

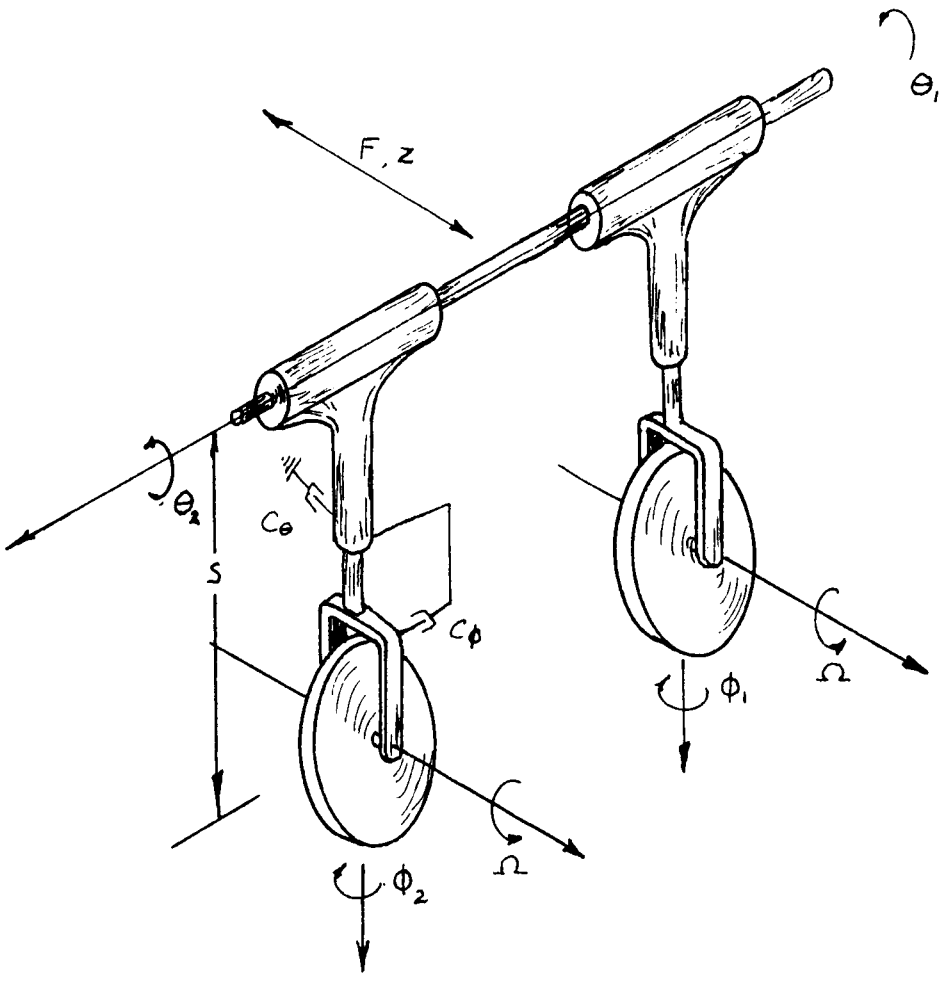

FIGURE 23.- PARALLEL GVA MOUNTING

Expanding this matrix yields the following response equation as for the single GVA:

$$\frac{\delta}{\delta_o}=\left\{\frac{\left[\frac{\omega^2}{\omega_a^2}-1\right]^2\left[\left(\frac{\omega^2}{\omega_a^2}-1-4\zeta_\theta\zeta_\phi\right)^2+\frac{\omega^2}{\omega_a^2}\left(2\zeta_\phi+2\zeta_\theta\right)^2\right]}{\left[\left(\frac{\omega^2}{\omega_a^2}-1\right)\left(\frac{\omega^2}{\omega_a^2}\left(1+\frac{2m}{M_c}-\frac{2S^2}{M\rho_\theta^2}\right)-\left(1+\frac{m}{M_c}\right)\right)+4\zeta_\theta\zeta_\phi\left(\frac{\omega^2}{\omega_a^2}\left(1+\frac{2m}{M_c}-\frac{S^2}{M\rho_\theta^2}\right)-\left(1+\frac{2m}{M_c}\right)\right)\right]^2+\frac{\omega^2}{\omega_a^2}\left[2\zeta_\theta\left(\frac{\omega^2}{\omega_a^2}\left(1+\frac{2m}{M_c}-\frac{S^2}{M\rho_\theta^2}\right)-\left(1+\frac{2m}{M_c}\right)\right)+2\zeta_\phi\left(\frac{\omega^2}{\omega_a^2}\left(1+\frac{2m}{M_c}-\frac{2S^2}{M\rho_\theta^2}\right)-\left(1+\frac{2m}{M_c}-\frac{S^2}{M\rho_\theta^2}\right)\right)\right]^2}\right\}^{\frac{1}{2}}$$

(83)

It can be seen (Figure 24) that even with damping on only one axis of one GVA, a zero response antiresonance and a damped resonant response are obtained. The damped resonant response will range from an infinite response for zero damping at a high frequency to an infinite response for infinite damping (on one GVA) at a lower frequency. These frequencies will be:

for the former,
$$\frac{\omega_G^2}{\omega_a^2}=\frac{1+2\mu}{1+2\mu\left(1-\frac{\rho_1^2}{\rho_\theta^2}\right)} \tag{84}$$

for the latter,
$$\frac{\omega_G^2}{\omega_a^2}=\frac{1+\frac{\mu}{1+\mu}}{1+\frac{\mu}{1+\mu}\left(1-\frac{\rho_1^2}{\rho_\theta^2}\right)} \tag{85}$$

At some intermediate damping and frequency there will be a minimum resonant response. This was borne out in the numerical analysis attendant to Figure 24 where it was found that a damping ratio, ζ_θ, of .05 yields a resonant response ratio of approximately 2.75.

For comparison, the response equation of a parallel Frahm mounting was derived, and it is as follows:

$$\frac{\delta}{\delta_o}=\frac{\left[\frac{\omega^2}{\omega_a^2}-1\right]\left[\left(\frac{\omega^2}{\omega_a^2}-1\right)^2+4\frac{\omega^2}{\omega_a^2}\zeta^2\right]}{\left[\frac{\omega^2}{\omega_a^2}-1\right]\left[\frac{\omega^2}{\omega_a^2}-1-2\mu\right]^2+4\frac{\omega^2}{\omega_a^2}\zeta^2\left[\frac{\omega^2}{\omega_a^2}(1+\mu)-1-2\mu\right]^2} \tag{86}$$

This is quite similar to the parallel GVA mounting. Here again, of course, it lacks the synchronizing capability of the GVA.

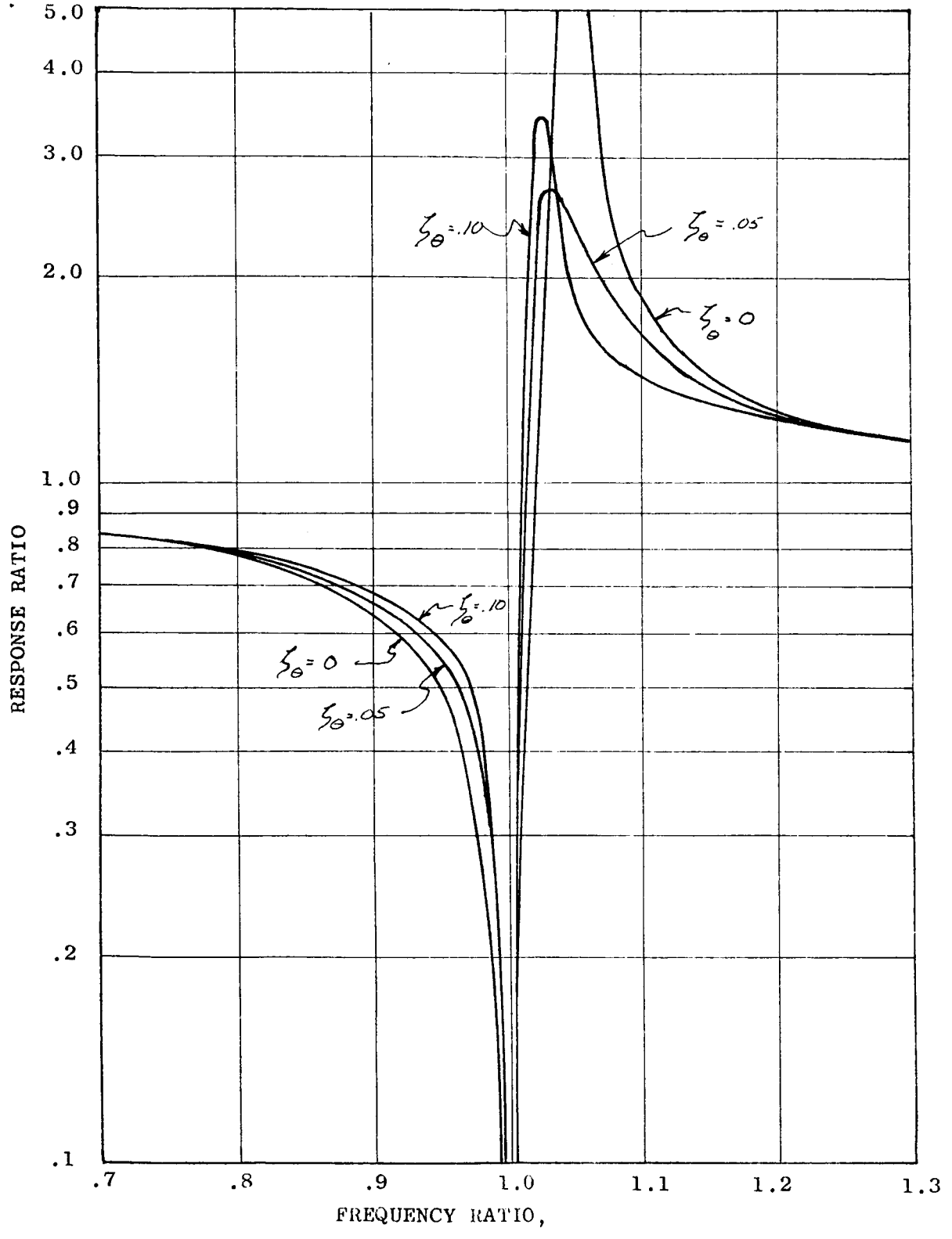

FIGURE 24.- RESPONSE RATIO VARIATION WITH FREQUENCY OF A PARALLEL GVA CONFIGURATION

Stability. - The dynamic stability was investigated for the parallel GVA using the Routh Criterion. The pertinent equation is that derived from the matrix on Page 51 , and is a quartic of the form:

$$S^4 + A_3 S^3 + A_2 S^2 + A_1 S + A_0 = 0 \tag{87}$$

where for stability, the complete criteria, as for the single GVA, is that all coefficients A are positive, and that:

$$\eta = \frac{A_1^2 + A_3 A_0}{A_1 A_2 A_3} < 1.0 \tag{88}$$

For the parallel GVA mounting:

$$\eta = \frac{(\eta_1 + \eta_2 \eta_3)^2 + \eta_1 (\eta_2 + \eta_3)^2 (\eta_3 4\zeta_\theta^2 + 1)}{\eta_2 (\eta_2 + \eta_3)(2 + \eta_3 4\zeta_\theta^2)(\eta + \eta_2 \eta_3)} \tag{89}$$

where:

$$\eta_1 = \frac{1 + 2\frac{m}{M_e}}{1 + 2\frac{m}{M_e}\left(1 - \frac{S^2}{2 I_\theta m}\right)} \tag{90}$$

$$\eta_2 = \frac{1 + 2\frac{m}{M_e}\left(1 - \frac{S^2}{2 I_\theta M_e}\right)}{1 - 2\frac{m}{M_e}\left(1 - \frac{S^2}{2 I_\theta M_e}\right)} \tag{91}$$

$$\eta_3 = \frac{\zeta_\varphi}{\zeta_\theta} \tag{92}$$

It can be determined from Equation (89), that since the coefficients A_0 through A_3 are positive for the parallel GVA, that with zero damping about either axis, θ or ϕ, there is positive stability for rotor speeds greater than zero.

Coriolis Absorber Configuration

Discussion. - Research on Kaman's Gyroscopic Vibration Absorber led to a synchronous absorber concept based on rotating inertial elements arranged in a manner different from the classical gyroscope. This rotating-inertia synchronous absorber (called the Coriolis Absorber because of the important role of Coriolis forces in its operation) has the advantages over the Gyroscopic Absorber of linear synchronization to two excitation frequencies and isotropic absorption in the plane of rotation.

The device, shown schematically in Figure 25, called the "Coriolis Absorber", will produce a response as shown in Figure 26 in all directions perpendicular to the axis of rotation. Figure 26 shows antiresonances at two frequencies which may or may not be harmonics. Figure 27 illustrates the Coriolis Absorber in motion. Figures 28 through 31 show alternate designs of the Coriolis Absorber.

Analysis of a mathematical model of the Coriolis Absorber shows that two sets of "tripoles" (such as shown in Figure 32), each set pivoting independently about one of the rotating axes, are sufficient for polar symmetry.

The fundamental analytical relationship between the gyroscopic and the "Coriolis" configuration is demonstrated by "position tensors",

where for the GVA,

$$\begin{vmatrix} X_f \\ Y_f \\ Z_f \end{vmatrix} = [\textcircled{H}][\Phi][\Psi] \begin{vmatrix} X_R \\ Y_R \\ Z_R \end{vmatrix} \qquad , \Omega = \frac{d\Psi}{dt}$$

and where for the Coriolis Vibration Absorber,

$$\begin{vmatrix} X_f \\ Y_f \\ Z_f \end{vmatrix} = [\Psi][\textcircled{H}] \begin{vmatrix} X_R \\ Y_R \\ Z_R \end{vmatrix} \qquad , \Omega = \frac{d\Psi}{dt}$$

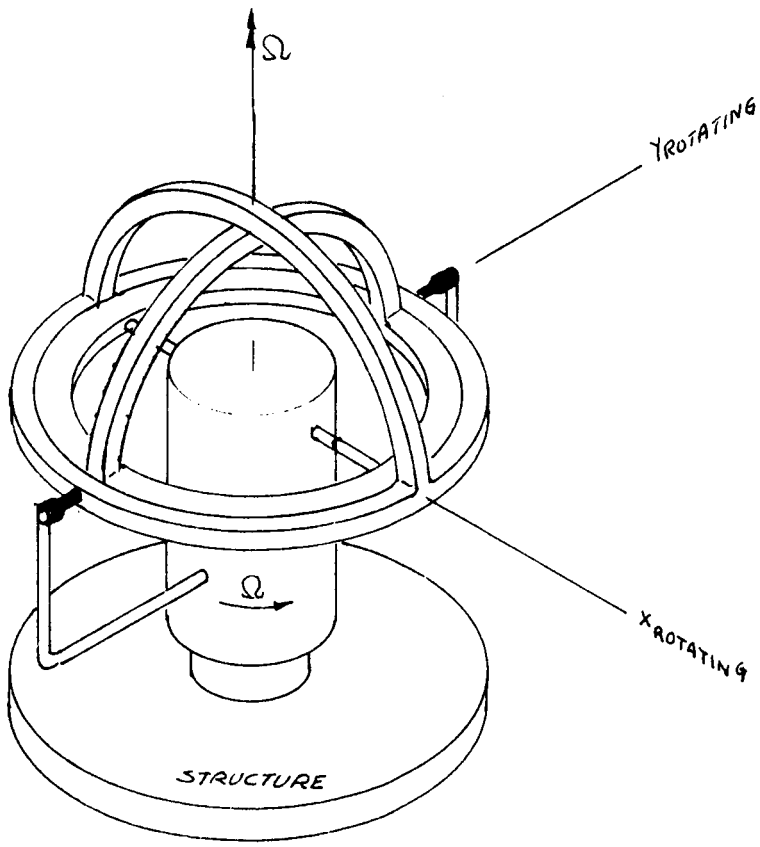

FIGURE 25.- SCHEMATIC OF KAMAN'S
CORIOLIS VIBRATION ABSORBER

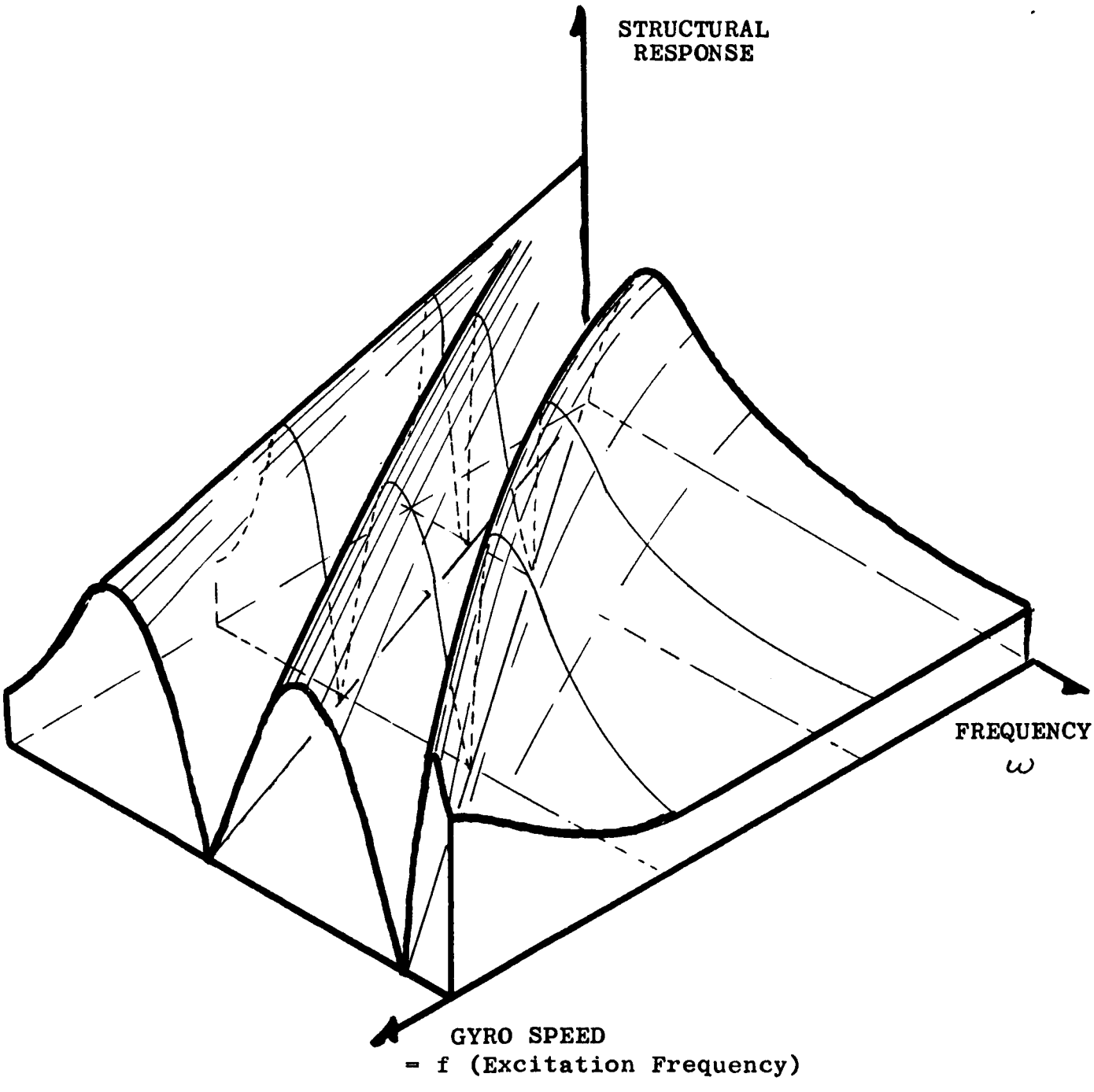

FIGURE 26. - GENERAL RESPONSE OF A
STRUCTURE WITH A CORIOLIS VIBRATION ABSORBER

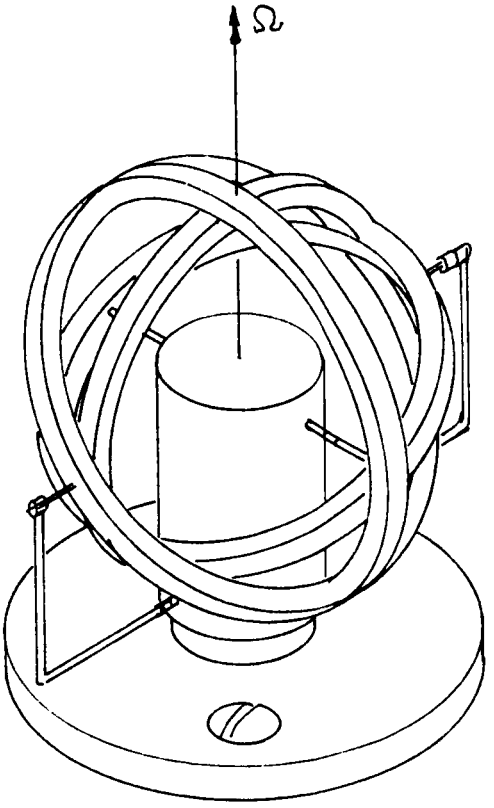

FIGURE 27.- CORIOLIS VIBRATION ABSORBER IN MOTION

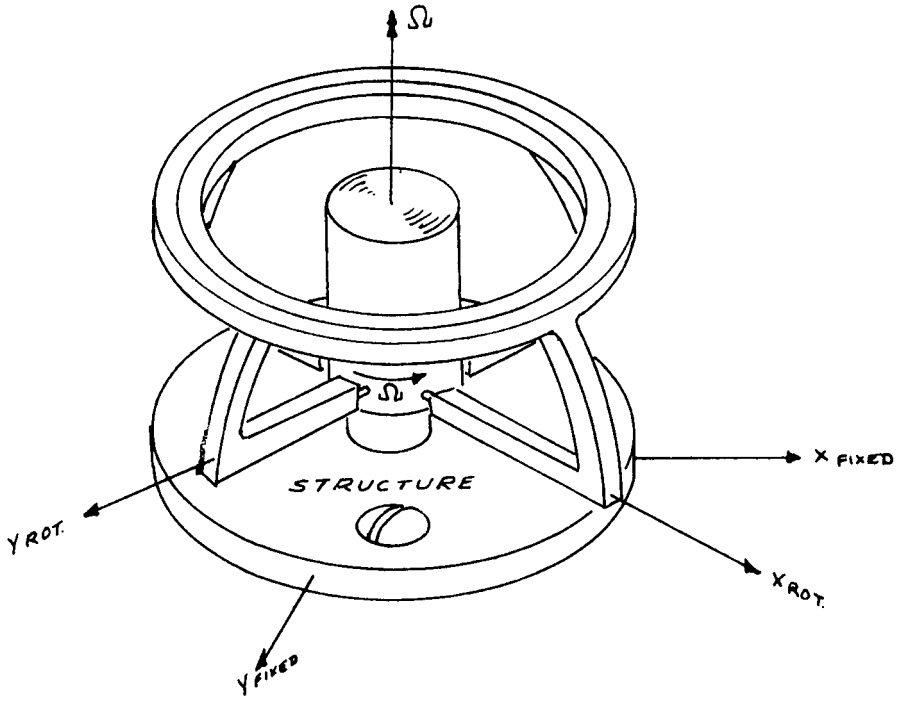

FIGURE 28.- AN ALTERNATE CONFIGURATION OF THE CORIOLIS VIBRATION ABSORBER

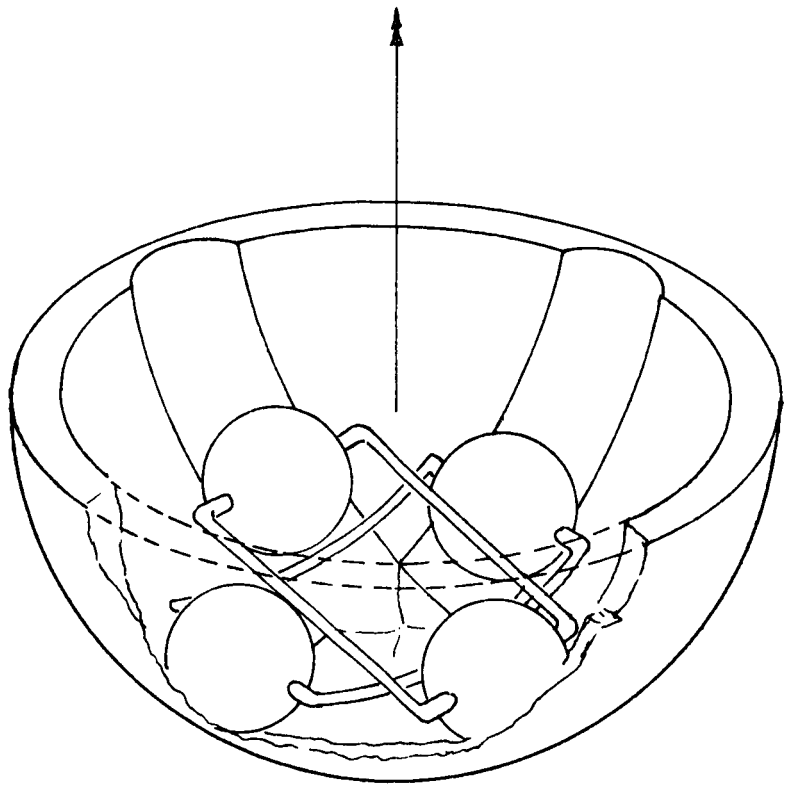

FIGURE 29.- AN ALTERNATE CONFIGURATION OF THE CORIOLIS VIBRATION ABSORBER

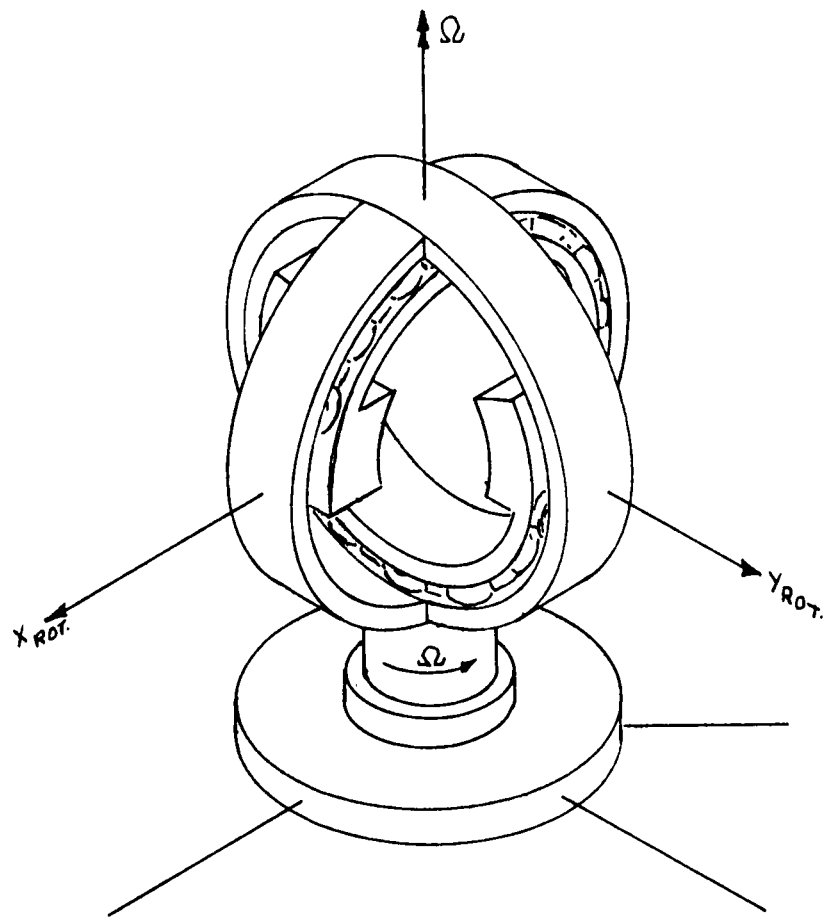

FIGURE 30.- AN ALTERNATE CONFIGURATION OF THE CORIOLIS VIBRATION ABSORBER

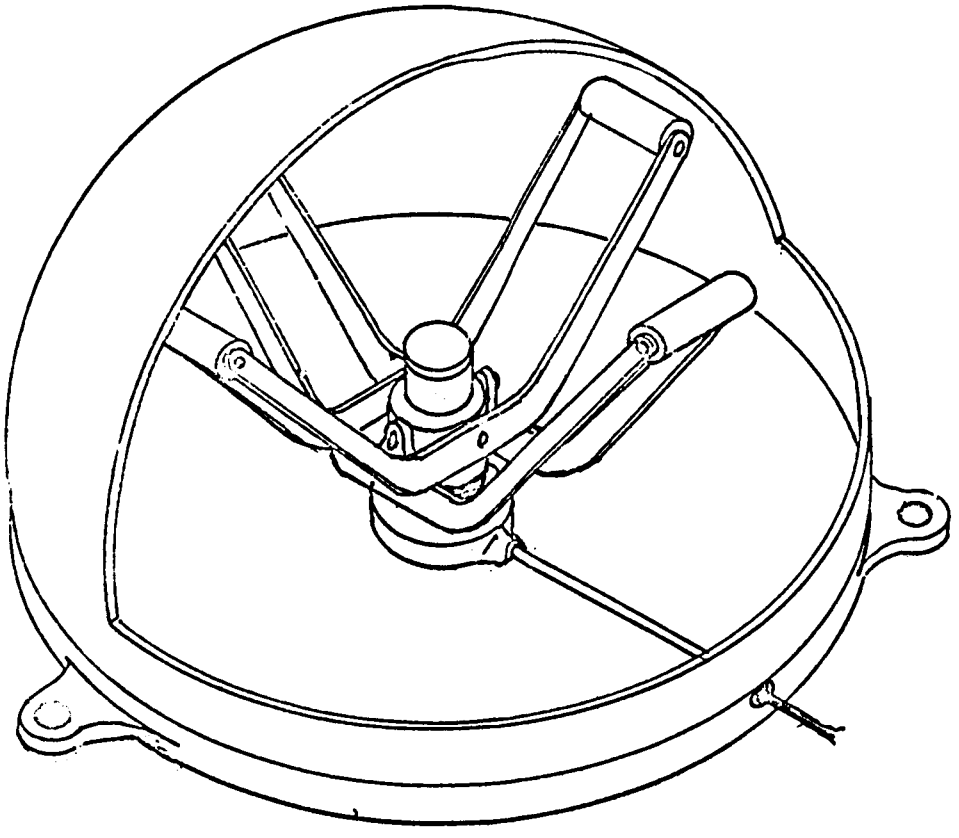

FIGURE 31.- AN ALTERNATE CONFIGURATION OF THE CORIOLIS VIBRATION ABSORBER

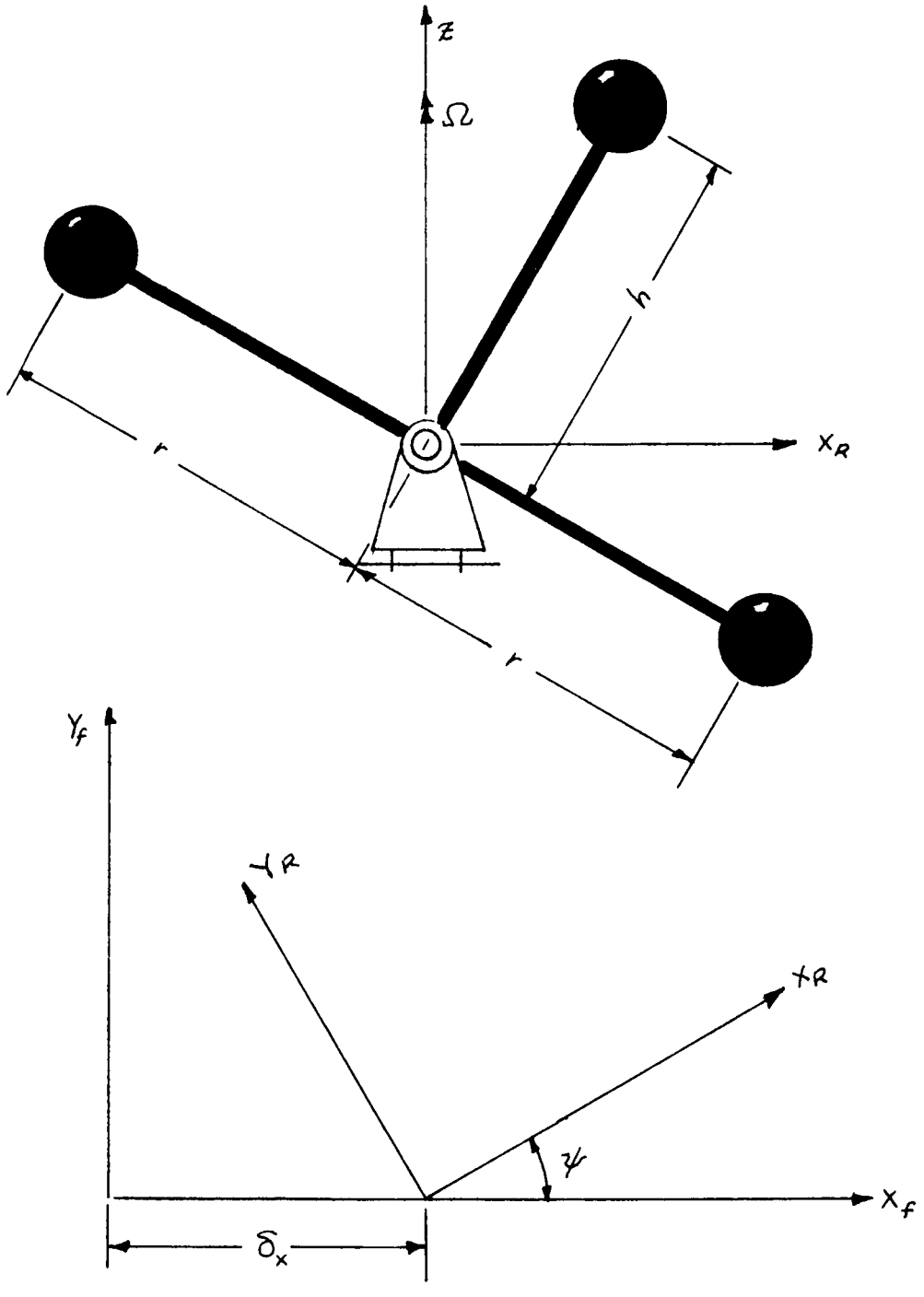

FIGURE 32.- TRIPOLE AXES SYSTEM

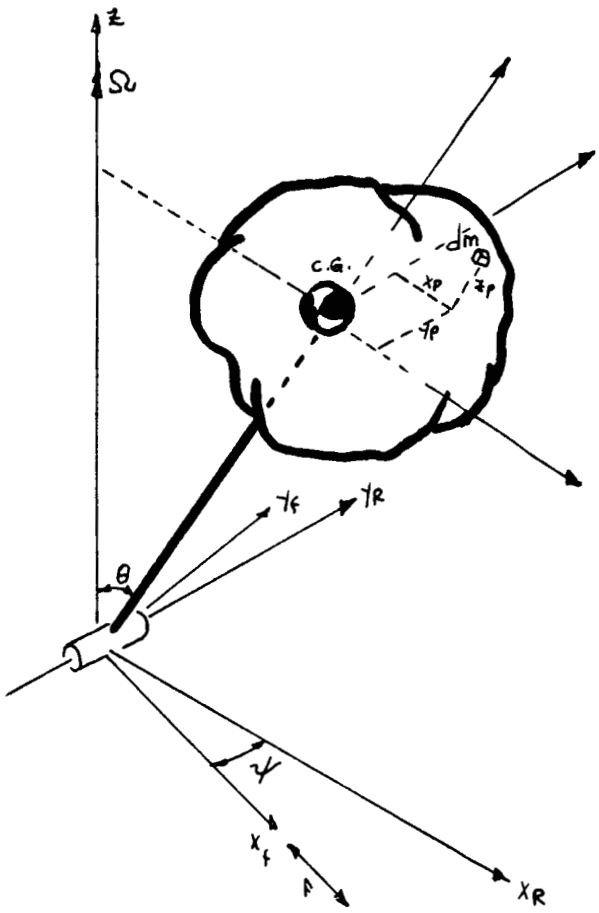

FIGURE 33.- GENERAL RIGID BODY AXIS SYSTEM

Analysis. - Consider a rigid body constrained to pivot about the γ_r axis with the center of gravity of the body a distance h from the γ_r axis. The coordinates x_p, y_p, z_p are fixed to the rigid body with the origin at the center of gravity and are principal axes. The fixed coordinates of a particle of the rigid body are given by Equations (93).

$$X_f = X_p(\cos\theta)(\cos\psi) - (Z_p - h)(\sin\theta)(\cos\psi) - Y_p(\sin\psi) + \delta_x$$

$$Y_f = Y_p(\cos\psi) + X_p(\cos\theta)(\sin\psi) - (Z_p - h)(\sin\theta)(\sin\psi) \qquad (93)$$

$$Z_f = Z_p(\sin\theta) + (Z_p + h)(\cos\theta)$$

Using the Principle of Virtual Work, d'Alembert's Equations for n identical rigid bodies disposed about the axis of rotation, each at angle ϕ_n from the Y_r axis, become:

$$\sum_{i=1}^{n} \int \left(\ddot{X}_f \frac{\partial X_f}{\partial \theta}\, dm\right)_i + \sum_{i=1}^{n} \int \left(\ddot{Y}_f \frac{\partial Y_f}{\partial \theta}\, dm\right)_i + \sum_{i=1}^{n} \int \left(\ddot{Z}_f \frac{\partial Z_f}{\partial \theta}\, dm\right)_i = 0 \qquad (94)$$

$$\sum_{i=1}^{n} \int \left(\ddot{X}_f \frac{\partial X_f}{\partial \delta_x}\, dm\right)_i + \sum_{i=1}^{n} \int \left(\ddot{Y}_f \frac{\partial Y_f}{\partial \delta_x}\, dm\right)_i + \sum_{i=1}^{n} \int \left(\ddot{Z}_f \frac{\partial Z_f}{\partial \delta_x}\, dm\right)_i = F_x$$

The second time derivatives of Equation (93) are:

$$\begin{aligned}
\ddot{X}_f = {} & -\ddot{\theta} X_p(\sin\theta)(\cos\psi) - \dot{\theta}^2 X_p(\cos\theta)(\cos\psi) + 2\Omega\dot{\theta} X_p(\sin\theta) \\
& - \Omega^2 X_p(\cos\theta)(\cos\psi) - (Z_p - h)(\ddot{\theta})(\cos\theta)(\cos\psi) + (Z_p - h)\dot{\theta}^2(\sin\theta)(\cos\psi) \\
& + 2(Z_p - h)\dot{\theta}\Omega(\cos\theta)(\sin\psi) + (Z_p - h)\Omega^2(\sin\theta)(\cos\psi) - \Omega^2 Y_p(\sin\psi) + \ddot{\delta}_x
\end{aligned}$$

$$\begin{aligned}
\ddot{Y}_f = {} & -Y_p\Omega^2(\cos\psi) - X_p\ddot{\theta}(\sin\theta)(\sin\psi) - X_p\dot{\theta}^2(\cos\theta)(\sin\psi) \\
& - 2X_p\Omega\dot{\theta}(\sin\theta)(\cos\psi) - X_p\Omega^2(\cos\theta)(\sin\psi) - (Z_p - h)\ddot{\theta}(\cos\theta)(\sin\psi) \\
& + (Z_p - h)\dot{\theta}^2(\sin\theta)(\sin\psi) - 2(Z_p - h)\dot{\theta}\Omega(\cos\theta)(\cos\psi) \\
& + \Omega^2(Z_p - h)(\sin\theta)(\sin\psi)
\end{aligned}$$

$$\ddot{Z}_f = X_p\ddot{\theta}(\cos\theta) - X_p\dot{\theta}^2(\sin\theta) - (Z_p + h)\ddot{\theta}(\sin\theta) - (Z_p + h)\dot{\theta}^2(\cos\theta) \qquad (95)$$

$$\frac{\partial X_f}{\partial \theta} = -X_p(\sin\theta)(\cos\psi) - (Z_p - h)(\cos\theta)(\cos\psi)$$

$$\frac{\partial Y_f}{\partial \theta} = -X_p(\sin\theta)(\sin\psi) - (Z_p - h)(\cos\theta)(\sin\psi)$$

$$\frac{\partial Z_f}{\partial \theta} = X_p(\cos\theta) - (Z_p + h)(\sin\theta) \qquad (96)$$

The partial derivatives of Equation (93) with respect to δ_x are all zero except:

$$\frac{\partial X_f}{\partial \delta_x} = 1 \tag{97}$$

Writing approximations for Equation (95) and Equation (96) for small values of angle θ, substituting into the first of Equation (91) and observing, in the integration, that axes p are principal axes, and the θ equation becomes:

$$\sum_{i=1}^{n} \left[(I_{z_p} - I_{x_i}) \Omega^2 \theta \right]_i + \sum_{i=1}^{n} (I_{y_i} \ddot{\theta})_i + \sum_{i=1}^{n} h^2 m \ddot{\delta}_x \cos(\psi + \phi_i) \cong 0 \tag{98}$$

Similarly, the δ_x equation becomes:

$$S_1 \sum_{i=1}^{n} \ddot{\theta} \cos(\psi + \phi_i) - 2 S_1 \sum_{i=1}^{n} \Omega \dot{\theta} \sin(\psi + \phi_i) - S_1 \Omega^2 \sum_{i=1}^{n} \theta \cos(\psi + \phi_i) + m \ddot{\delta}_x \cong F_x$$

where $S_1 = hm$ and m is the total mass of the rotating elements.

Multiplying Equation (98) by sin $(\Omega t + \phi_i)$ and again by cos $(\Omega t + \phi_i)$ to yield two equations with fixed system coordinates, and making the substitutions:

$$\xi_1 = \sum_{i=1}^{n} \theta \sin \psi_i$$

$$\dot{\xi}_1 = \sum_{i=1}^{n} \dot{\theta} \sin(\Omega t + \phi_i) + \Omega \sum_{i=1}^{n} \theta \cos(\Omega t + \phi_i)$$

$$\ddot{\xi}_1 = \sum_{i=1}^{n} \ddot{\theta} \sin(\Omega t + \phi_i) + 2\Omega \sum_{i=1}^{n} \dot{\theta} \cos(\Omega t + \phi_i) - \Omega^2 \sum_{i=1}^{n} \theta \sin(\Omega t + \phi_i) \tag{100}$$

and also the substitutions:

$$\xi_2 = \sum_{i=1}^{n} \theta \cos(\Omega t + \phi_i)$$

$$\dot{\xi}_2 = \sum_{i=1}^{n} \dot{\theta} \cos(\Omega t + \phi_i) - \Omega \sum_{i=1}^{n} \theta \sin(\Omega t + \phi_i)$$

$$\ddot{\xi}_2 = \sum_{i=1}^{n} \ddot{\theta} \cos(\Omega t + \phi_i) - 2\Omega \sum_{i=1}^{n} \dot{\theta} \sin(\Omega t + \phi_i) - \Omega^2 \sum_{i=1}^{n} \theta \cos(\Omega t + \phi_i) \tag{101}$$

and summing for n = 2, $\phi_2 = \frac{\pi}{2}$, it is seen that:

$$
\begin{aligned}
&I_{y_1}\left(\ddot{\xi}_{1_1} - 2\Omega\dot{\xi}_{1_2} - \Omega^2\xi_{1_1}\right) + (I_2 - I_{x_1})\,\Omega^2\xi_{1_1} = 0 \\
&I_{y_1}\left(\ddot{\xi}_{1_2} + 2\Omega\dot{\xi}_{1_2} - \Omega^2\xi_{1_2}\right) + (I_2 - I_{x_1})\,\Omega^2\xi_{1_2} + S_1\ddot{\delta}_x = 0 \\
&S_1\ddot{\xi}_{1_2} + m\ddot{\delta}_x = F_x
\end{aligned}
\tag{102}
$$

and the equations of motion of the system.

In matrix form:

$$
\begin{bmatrix}
0 & -\omega^2 I_{x_1} + \Omega^2(I_2 - I_{x_1} - I_{y_1}) & -2i\omega\Omega I_{y_1} \\
-S_1\omega^2 & 2i\omega\Omega I_{y_1} & -\omega^2 I_{y_1} + \Omega^2(I_2 - I_{x_1} - I_{y_1}) \\
-m\omega^2 & 0 & -S_1\omega^2
\end{bmatrix}
\begin{vmatrix} \delta_x \\ \xi_{1_1} \\ \xi_{1_2} \end{vmatrix}
=
\begin{vmatrix} 0 \\ 0 \\ F \end{vmatrix}
\tag{103}
$$

Using Cramer's Rule,

$$
\frac{\delta_x}{F} = \frac{-\omega^2 4\Omega^2 I_{y_1}^2 + \left[\omega^2 I_{y_1} - \Omega^2(I_2 - I_{x_1} - I_{y_1})\right]^2}{m\omega^4(I_{x_1}h^2 m + I_{x_1}^2) + \omega^2\left[4\Omega^2 I_{y_1}^2 + \Omega^2(I_2 - I_{x_1} - I_{y_1})(2I_{x_1} - h^2 m)\right] + \Omega^4(I_2 - I_{x_1} - I_{y_1})^2}
\tag{104}
$$

$\delta_x = 0$ when

$$
\pm 2\omega\Omega I_{y_1} = \omega^2 I_{y_1} - \Omega^2(I_2 - I_{x_1} - I_{y_1})
$$

and the antiresonant frequencies are given by:

$$
\boxed{\omega_a = \Omega\left[1 \pm \sqrt{\frac{I_2 - I_{x_1}}{I_{y_1}}}\right]}
\tag{105}
$$

Note that there are two antiresonances, each antiresonant frequency directly proportional to the angular velocity of the absorber.

Setting the denominator of Equation (104) equal to zero and solving for ω shows that there are two resonant frequencies.

The summations for two rigid masses, performed on Equations (100) and (101) in obtaining Equation (102), show that the absorber has polar symmetry about the axis of rotation.

RANDOM VIBRATION APPLICATIONS

The GVA is superior to the Frahm absorber in the attenuation of a random vibration spectrum, since synchronization of the GVA to the predominant frequency or frequency band is feasible. Where such a frequency is a function of some "shaft" speed, a generator could be driven directly by the shaft, thus supplying to the GVA rotor a driving frequency proportional to the shaft speed. However, where the predominant frequency is not such a direct function, then electronic discriminatory circuitry must be employed. Its purpose would be to survey a time history of acceleration obtained with a band-pass filter (or spectrum analyzer) fed by a vibration transducer. The survey of power versus frequency will yield a signal input to control the GVA rotor speed such that the antiresonance will occur at the frequency of maximum power spectral density.

Since power spectral densities of input, $x(\omega)$, and response $y(\omega)$, are related by the following expression (Reference 7):

$$x(\omega) = Y(\omega)\left[\frac{\delta}{\delta_0}\right]^2 \tag{106}$$

it can be seen that there is slight difference between the conventional Frahm and the GVA (linearized response) if both are tuned to the same frequency. However, slight changes in the predominant frequency negates the effectiveness of the Frahm, whereas the GVA can be resynchronized.

CONCLUSIONS

1. Rigorous derivation of the equations of motion of the GVA confirms that the antiresonance can be linearly synchronized to the excitation frequency, thereby giving the effect of infinite bandwidth to a discrete but variable excitation antiresonant frequency.

2. The capacity of the GVA to produce an antiresonance, the frequency of which is a function of gyro speed, was demonstrated experimentally.

3. Preliminary analysis indicates that a particular configuration of synchronous absorbers is capable of simultaneous synchronization of two antiresonant frequencies and will produce antiresonance in any direction in the plane of rotation.

4. The mounting of two GVA's in parallel, one damped and the other undamped, yields (from the linearized equations) an undamped antiresonant frequency and a damped resonance which can be optimized.

5. Torsional spring restraint about either the θ or ϕ axis of the GVA causes a finite antiresonant frequency at zero gyro speed. However, the antiresonant frequency asymptotically approaches linearity with gyro speed as the gyro speed becomes very large compared to the static (nonrotating) natural frequency.

6. Torsional restraint about both the θ and ϕ axes of the GVA produces two antiresonances, one of which asymptotically approaches zero while the other asymptotically approaches linearity with gyro speed as the gyro speed becomes large compared to the nonrotating natural frequency.

7. Damping about either axis of the GVA, θ or ϕ, should be minimized for minimum structural response at antiresonance.

8. Structural flexibility in the tare (or inner gimbal) of the GVA causes the antiresonant frequency to asymptotically approach a finite value which is always less than the nonrotating "beam" mode frequency of the GVA. This phenomenon is an example of translatory environmental excitation of gyroscopic nutational resonance.

9. A method of solving the exact equations of motion, including the effects of damping and elastic restraint, is presented.

10. The absorption by the GVA of a spectrum of random vibration is similar to that of a conventional Frahm when tuned to the same frequency. However, synchronization to a variable power peak in that spectrum is feasible for the GVA.

REFERENCES

1. Den Hartog, J. P., "Mechanical Vibrations", 4th Edition, McGraw-Hill Publishing Company, New York, 1956

2. Jones, R. and Ellis, C. W., "Application of an Absorber to Reduce Helicopter Vibration Levels", Journal of the American Helicopter Society, July, 1963

3. Thompson, J. R. and Yeates, J. E., "A Limited Flight Investigation of the Effect of Dynamic Vibration Absorbers on the Response of an Airplane Structure Buffeting", NACA RM L54K02, 25 January 1955

4. Arnold, R. N. and Maunder, L., "Gyrodynamics and Its Engineering Applications", Academic Press, London, 1961

5. Flannelly, W. G., "Gyroscopic Vibration Absorber Test Report", Kaman Aircraft Corporation Report AIR 63-4, 30 August 1963

6. Flannelly, W. G., "Gyroscopic Vibration Absorber Research Proposal", Kaman Aircraft Corporation Report No. R-499, 26 March 1963

7. Piersol, A. G., "The Measurement and Interpretation of Ordinary Power Spectra for Vibration Problems", NASA Contractor Report NASA CR-90, September, 1964

8. Reed, F. E., "The Use of the Centrifugal Pendulum Absorber for the Reduction of Linear Vibration", Journal of Applied Mechanics, Volume 19, Page 190, 1949

9. Laufer, T., "A Vibration Absorber for Two-Bladed Helicopters", NASA TT F-43, November, 1960

10. Lynn, Robert R., "Dynamic Absorbers in the Rotating System of Helicopters", IAS Paper No. 60-28, January, 1960